MODELING OF FLAT-PLATE SOLAR COLLECTOR OPERATION IN TRANSIENT STATES

A Thesis

Submitted to the Faculty

of

Purdue University

by

Ahmad M. Saleh

In Partial Fulfillment of the

Requirements for the Degree

of

Master of Science in Engineering

May 2012

Purdue University

Fort Wayne, Indiana

شُكراً

To my wife and my soul mate, RANA, you are the light of my life

To the smile of my life, to my big boy, LAITH

To my father and mother, to whom I will be grateful forever

To my sisters, All'a and Reem; my brothers, Mahmoud and Mohammed

ACKNOWLEDGMENTS

The author would like to extend his thanks to his advisors Dr. Hosni Abu-Mulaweh and Dr. Donald Mueller, for their excellent guidance and encouragement throughout the study.

The author would like to thank Dr. Peter Dragnev and Dr. Zhuming Bi for the interest they have shown in the study by being members of the examining committee and for their helpful comments.

The author is grateful to Dr. Suliman Ashur and Dr. Mohammed Alhassan: a special thank for all your encouragement, support, guidance, and valuable advice.

Finally, I would like to extend my thanks to all persons who encouraged or helped me during my work, especially: R. Amayreh, L.Amayreh, B. Nuaerat, M. Saleem, A. Izmirly, A. Abu-Aqeel, M. Dafua, M. Kadous, Y. Mahmat, and R. Fares.

TABLE OF CONTENTS

Page

Page

LIST OF TABLES

LIST OF FIGURES

Figure Page

NOMENCLATURE

Notations

A	Flow rate (m^2)
c	Specific heat (J/(Kg.K))
d	diameter of the collector tube (m)
G	Heat flux of solar radiation (W/m^2)
h	Heat transfer coefficient ($W/(m^2.K)$)
i	specific enthalpy (J/Kg)
k	Thermal conductivity (W/(m.K))
L	length of the analyzed collector (m)
$\dot{m}$	Mass flow rate (Kg/s)
M	Number of nodes perpendicular to the flow direction
n	Number of solar collector tubes
N	Number of cross-sections (nodes in flow direction)
p	tube pitch (m)
r	radius of the collector tube (m)
T	Temperature (K)
V	Volume (m^3)
w	Flow velocity (m/s)
z	Spatial co-ordinate (m)
α	Absorption coefficient
β	Collector inclination angle (rad)
δ	Thickness (m)
$\Delta\tau$	Time step (s)
Δz	spatial size of control volume (m)
ε	Emissivity
ρ	Density (Kg/m^3)
σ	Stefan-Boltzmann constant ($W/(m^2 K^4)$)
τ	time (sec)
$(\tau\alpha)$	effective transmittance-absorption coefficient

Subscripts

a	air gap between glass cover and absorber
ab	absorber
am	ambient
c	convection
f	working fluid
g	glass cover
i	insulation
in	inner
j	subsequent control volume
o	outer
r	radiation
t	total

ABSTRACT

Saleh, Ahmad M. M.S.E., Purdue University, May 2012. Modeling Of Flat-Plate Solar Collector Operation in Transient States. Major Professor: Hosni Abu-Mulaweh.

Solar energy is becoming an alternative for the limited fossil fuel resources. One of the simplest and most direct applications of this energy is the conversion of solar radiation into heat, which can be used in water heating systems. A commonly used solar collector is the flat-plate. A lot of research has been conducted in order to analyze the flat-plate operation and improve its efficiency. This study presents a one-dimensional mathematical model for simulating the transient processes which occur in liquid flat-plate solar collectors. The proposed model simulates the complete solar collector system including the flat-plate and the storage tank. The model considers time-dependent thermo-physical properties and heat transfer coefficients and is based on solving equations which describe the energy conservation for the glass cover, air gap between cover and absorber, absorber, working fluid, insulation, and the storage tank. The differential equations were solved using the implicit finite-difference method in an iterative scheme and executed using the MATLAB. In order to verify the proposed method, an experiment was designed and conducted for several days with variable ambient conditions and flow rates. The comparison between the computed and measured results of the transient fluid temperature at the collector outlet showed a satisfactory

convergence. The proposed method is an appropriate for the verification of the absorber and glass cover effectiveness, and to calculate the overall efficiency of the system along with the overall heat loss factor.

CHAPTER 1- INTRODUCTION

1.1 General

Due to environmental issues and limited fossil fuel resources, more and more attention is being given to renewable energy sources. A new government study shows that Americans are using less energy overall and making more use of renewable energy resources.

The United States used significantly less coal and petroleum in 2009 than in 2008, and significantly more renewable power. There also was a decline in natural gas use and increases in solar, hydro and geothermal power according to the most recent energy flow charts released by the Lawrence Livermore National Laboratory, figure 1.1.

The Annual Energy Review 2010, done and published by the U.S Energy Information Administration shows that the renewable energy's market share reached 8 percent of total U.S. energy consumption, as total consumption decreased nearly 5 percent while renewable energy consumption rose 5 percent. Total renewable energy consumption rose from 7.4 to 7.7 quadrillion Btu. Figure 1.2 presents the renewable Energy consumption by major source for 2010.

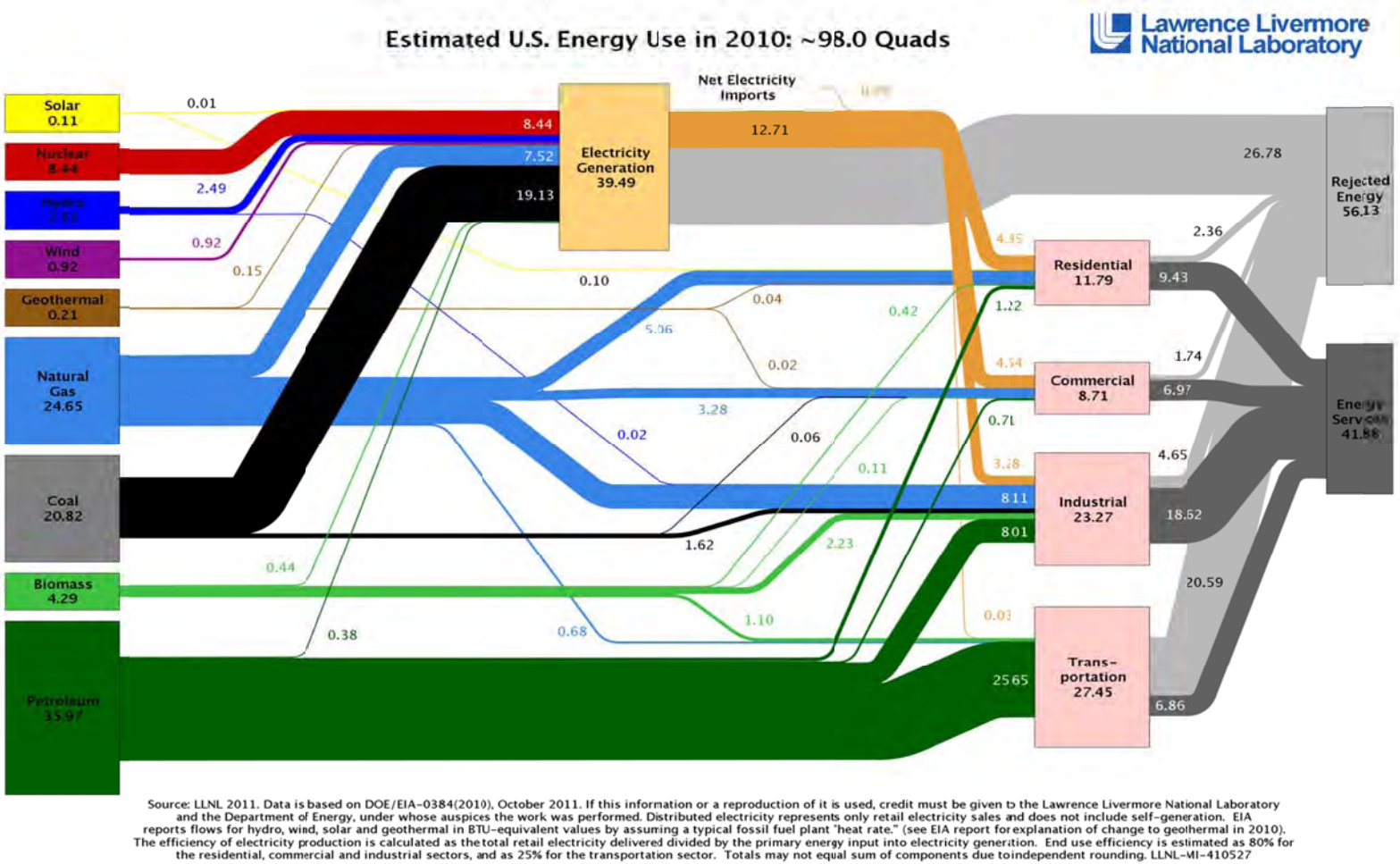

Figure 1.1: Estimated U.S Energy Use in 2010
[http://www.renewableenergyworld.com]

:

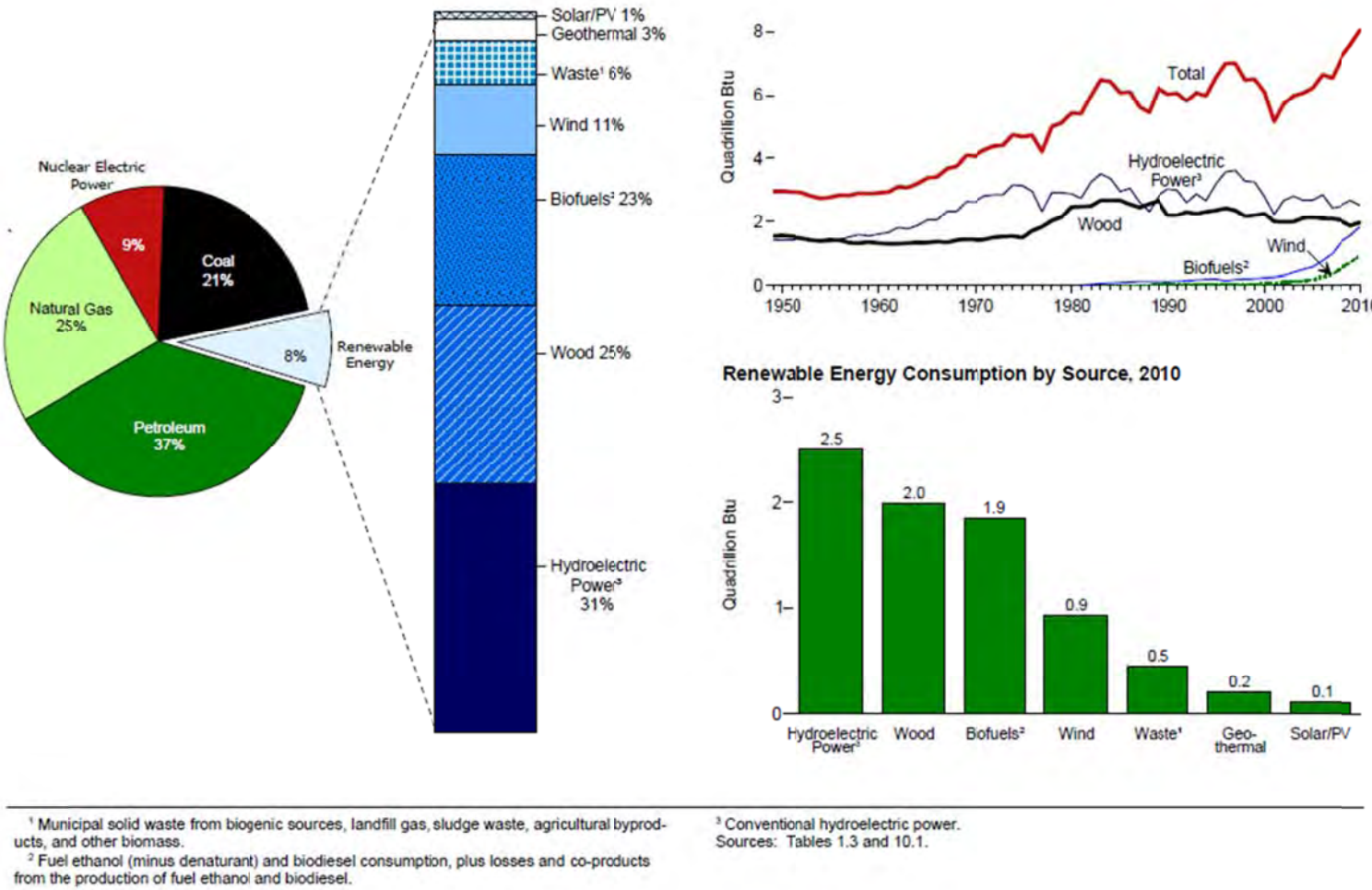

¹ Municipal solid waste from biogenic sources, landfill gas, sludge waste, agricultural byproducts, and other biomass.
² Fuel ethanol (minus denaturant) and biodiesel consumption, plus losses and co-products from the production of fuel ethanol and biodiesel.
³ Conventional hydroelectric power.
Sources: Tables 1.3 and 10.1.

Figure 1.2: Renewable Energy Consumption by Major Source.
[U.S. Energy Information Administration / Annual Energy Review 2010]

In the recent years solar energy has been strongly promoted as a viable energy source. One of the simplest and most direct applications of this energy is the convergence of solar radiation into heat.

Solar radiation can be widely used for water heating in hot water systems, swimming pools as well as a supporting energy sources for central heating installations. The energy of the solar radiation is in this case converted to heat with the use of solar panel, Zima and Dziewa, [2010]. Using the sun's energy to heat water is not a new idea. More than one hundred years ago, black painted water tanks were used as simple solar water heaters in a number of countries. However, the solar water heating technology has greatly improved during the past century. Today there are more than 30 million square meters of solar collectors installed around the globe, RETScreen [2012].

Most solar water heating systems for buildings have two main parts: a solar collector and a storage tank. Solar collectors are the key component of solar-heating systems. They gather the sun's energy, transform its radiation into heat, and then transfer that heat to a fluid (usually water or air).

Solar water heating systems can be either active or passive, but the most common are active systems. Active systems rely on pumps to move the liquid between the collector and the storage tank, while passive systems rely on gravity and the tendency for water to naturally circulate as it is heated. Figure 1.3 shows the schematic of a typical active solar system employing a flat plate solar collector and a storage tank. With Q_i is the amount of solar radiation received by the collector. As the collector absorbs heat its temperature is getting higher than that of the surrounding and heat is lost to the atmosphere by convection and radiation, this heat loss rate presented by Q_o.

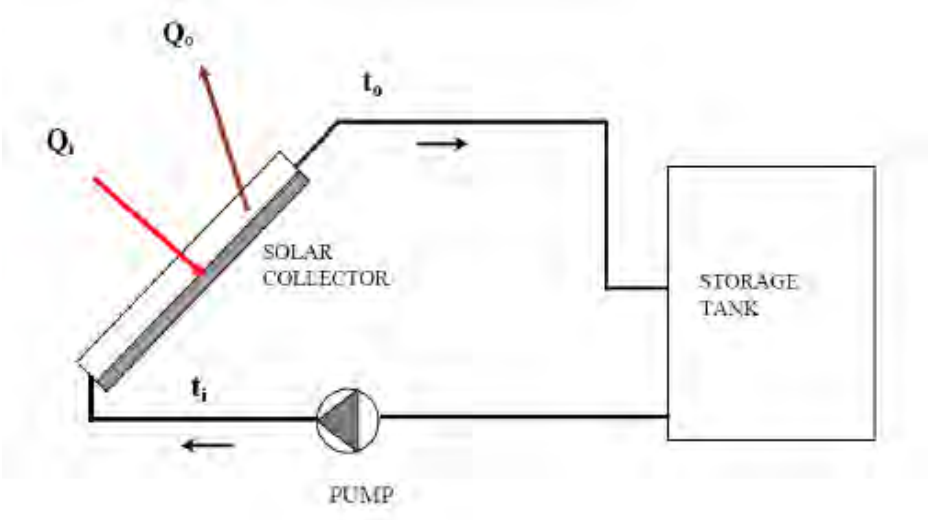

Figure 1.3: Typical active solar energy collection system

There are a large number of solar collector designs that have shown to be functional; these designs are classified in two general types of solar collectors:

- Flat-plate collectors – the absorbing surface is approximately as large as the overall collector area that intercepts the sun's rays.
- Concentrating collectors – large areas of mirrors or lenses focus the sunlight onto a smaller absorber, Figure 1.4.

Flat-plate collectors are the most common solar collector for solar water-heating systems in homes and solar space heating. A typical flat-plate collector, figure 1.5, consists of an absorber in an insulated box together with transparent cover sheets (glazing). The absorber is usually made of a metal sheet of high thermal conductivity, such as copper or aluminum, with integrated or attached tubes. Its surface is coated with a special selective material to maximize radiant energy absorption while minimizing radiant energy emission. The insulated box reduces heat losses from the back and sides of the collector. These collectors are used to heat a liquid or air to temperatures less than

80°C, Srutckmann, [2008]. The performance and operation of a flat-plate collector is governed by the fundamental laws of thermodynamics and relationships from heat transfer and fluid mechanics.

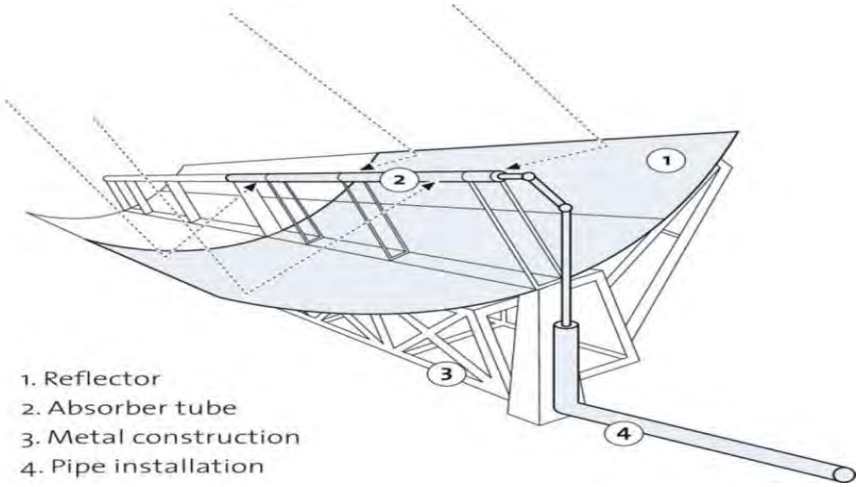

Figure 1.4: Schematic of a Concentrating Solar Collector
[http://asolarheater.net/1198-solar-trough-collectors.html]

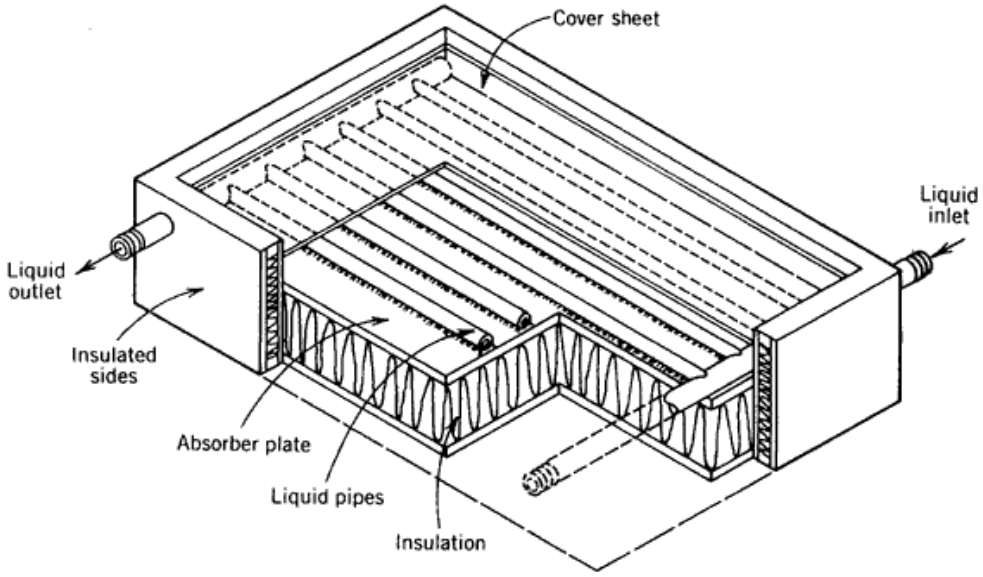

Figure 1.5: Cross-section of a typical liquid flat plate collector

The research in this thesis is concerned with the mathematical modeling of the flat-plate solar collector working under transient conditions. This is done by deriving governing equations for each layer in the solar collector (cover, air gap, absorber, working fluid, and insulation), the derived model will be solved using an implicit finite difference method in an iterative scheme utilizing the MATLAB software.

The proposed solution method numerically solves the derived model considering all the transient conditions in the collector's process, and computes the transient temperature distributions for any cross-section at the collector.

As a verification of the proposed solution method; an experimental work has been done on an active flat-plate solar collector, all the experiments has been performed at the laboratory facilities of the engineering department in Indiana-Purdue University- Fort Wayne. The experimental results were compared to the temperatures obtained by the MATLAB code.

1.2 Objectives

The main objectives of this study are:

1. To develop a dynamic mathematical model for an active flat-plate solar collector with single glass cover working in parallel channel arrangement under transient conditions.
2. Propose a solution method to the derived model has the capability to compute the transient temperature distributions for any cross-section at the collector at any certain time.

3. Utilize the MATLAB software to generate a code that can numerically apply the proposed solution method.
4. Experimentally verify the proposed solution method for the derived model.

1.3 Thesis Organization

The thesis consists of seven chapters, chapter one presents the introduction.

Chapter two is review of the theoretical and experimental works done in order to analyze and modeling the solar collector.

Chapter three presents the detailed derivation of the mathematical model that portrays the operation of a flat-plate solar collector under transient conditions and the proposed method used to solve this model.

Chapter four describes the developed MATLAB code used to numerically solve the proposed solution method, along with an illustration of the code inputs and outputs.

Chapter five presents the experimental work conducted in this study. It includes a detailed description of the experiment setup and the experimental procedures that were done.

Chapter six presents the analysis and discussion to the experimental results. Comparison between the experimental results and the computed value will also be presented in this chapter to evaluate the derived model and the proposed solution method.

Chapter seven provides the conclusions and recommendations.

CHAPTER 2- LITERATURE REVIEW

There is an increasing demand for the solar collectors, especially the flat-plate liquid solar collector. Therefore, an extensive research has been done to model the flat-plate solar collector's operation and to predict the performance of different types solar collector. This chapter presents a summary of the fundamentals as well as the state-of-the-art research that has been conducted in the area of flat-plate solar collector modeling and performance prediction.

Owing to the many parameters affecting the solar collector performance, attempting to make a detailed analysis of a solar collector is a very complicated problem. Fortunately, a relatively simple analysis will yield very useful results, Duffie Beckmann [1991]. Mainly there are two general test methods have been followed in analyzing the flat-plat solar collector performance: the stationery test and the dynamic solar collector model. Dynamic models were initially based on a one-node model. This kind model attempts to include the effects of thermal capacitance in a simple fashion. The one-node model was then upgraded to multi-node model was introduced, considering the collector consists of multiple nodes each with a single temperature and capacitance. The assumption of steady-state conditions (constant inlet temperature, fluid flow rate in pipes, incident irradiance and ambient conditions) in the stationary methods makes the collector tests much complicated and more expensive. Since normally solar collectors operate at

transient conditions (outdoor ambient), the steady state test conditions are not typical of normal operation.

The solar collector's stationary models presented by Hottel and Woertz [1942], Hottel and Whillier [1985] and Bliss [1959] were based on a zero-capacitance model, the effects of thermal capacitance on the collector performance are neglected. The collector is considered to be in equilibrium with its environment at any instant time. A single value of the collector overall loss coefficient is considered in the model, independent of the continuously variable ambient conditions.

A test method that incorporates dynamic solar collector properties not only yields more information about the collector, but makes collector testing easier to perform experimentally. Thus, testing is made less expensive, while the model and the computation procedures will be more complex. However, the model and the computation procedure must be developed only once, while experimental expense must be made for each test, Muschaweck [1993].

In an effort to include the capacitance effects on the collector performance, Close [1967] developed the one-node capacitance model. In which he assumes that the capacitance is all lumped within the collector plate itself. The limitations of this model are the assumptions that the temperature distribution along the flow direction is linear, and the fluid and tube base are at the same temperature. This model has been shown to be useful in predicting the performance of the collector including the collector storage effect due to the thermal capacitance. To determine the transient effect of thermal capacitance, a more complicated model is needed.

The working conditions of the solar collector are unavoidably transient and non-uniformity flow is present; therefore the need for a transient and multidimensional model arises. However, a detailed model analysis considers these aspects gives complicated governing equations that are difficult to solve. Therefore different models with simplified assumptions were developed in an attempt to predict the solar collector performance under transient conditions.

Klein et. al. [1974] suggested a 2-node model in which nodes are positioned at the collector plate and at a single glass cover. The collector mean temperature assumed to be the algebraic average of the inlet and outlet fluid temperatures. In their study, they used a first and a second order differential equations to describe the collector. But, in essence, a collector is a distributed system and hence would merit a description by one or more partial differential equations.

De Ron [1980] presented a dynamic model of a single glass cover flat-plate collector. Adding to assumptions made by Duffie [1974]. In his model, he made the following assumptions:

1. All heat transport phenomena are taken in 1-D perpendicular to the flow direction, except for the heat carried by the flow.
2. The temperature gradients in the thickness of the cover and the absorber are negligible.
3. The heat flow into the insulation at the back is negligible.
4. Perfect insulation at the edges.
5. The heat capacity of the air gap between the cover and the absorber plate is neglected.

De Ron represented the cover and the absorber energy balances by an ordinary differential equation, while the fluid temperature described by a partial differential equation. Although the derived model was nonlinear, using Taylor series expansion around the average operating conditions, a linear approximation was obtained. The model is not valid for large range of disturbance for the wind speed and flow variations.

Kamminga [1985] derived analytic approximations of the temperatures within a flat-plate solar collector under transient conditions. Based on the fact that some of the heat resistances of a conventional flat-plate solar collector are smaller than others, Kamminga derived a 4-nodes mathematical model (cover, absorber, fluid and insulation). The model approximates the temperatures of the collector at any certain time using the measured ambient, insulation, and fluid outlet temperatures. However, the method used to solve the model is not suitable for variable flow rates.

Wang and Wu [1990] proposed a discrete numerical model to calculate the flow and temperature distribution to analyze the performance of flat-plate solar collector arrays. For large Z- arranged collector arrays, in which the flows are parallel in the dividing and combining manifolds as shown in figure 2.1, the numerical model showed high agreement with the measured experimental data. A number of simplified assumptions were made:

1. Flow distribution among branch pipes may not be uniform.
2. Fluid properties are independent of temperature except density; the buoyancy effect cannot be neglected.
3. Longitudinal heat conduction in absorber plate and pipe wall cannot be neglected.
4. Heat transfer in manifolds cannot be neglected.

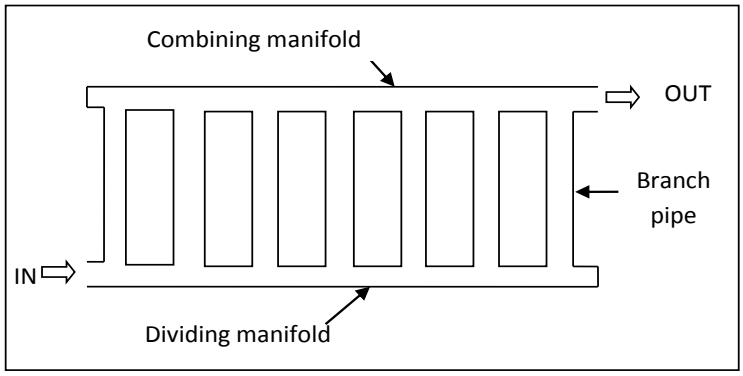

Figure 2.1: Z-arranged collector array.

However, the model requires a constant inlet temperature and constant flow rate during the test. According to Their results the flow non-uniformity has detrimental effects on the thermal performance of collector array, the use of the Hottel, Whillier, Bliss model (HWB model) presented by Duffie [1980] to predict the performance of large collector array may cause large error.

Oliva et al. [1991] introduced a numerical method to determine the thermal behavior of a solar collector. The distributed-character model considers the multidimensional and transient heat transfer properties that characterize the solar collector, while the flux of heat transfer by free convection at the air gap zone has been evaluated using empirical expressions and the solar irradiance was integrated to be constant hourly. The analysis has been done specifically for an air collector with rectangular ducts. Although the presented model was done in a physically almost exact way; it is hard to be implemented in practice.

Muschawec and Spirkl [1993] presented a dynamic solar collector model in conjunction with a dynamic parameter identification and performance prediction method. The parameter identification method developed by Spirkl [1990] was used in conjunction

with a collector model instead of the solar domestic hot water (SDHW). The model used extends the Hottel –Whillier–Bliss equation presented in Dufie and Beckmann [1991] to a dynamic one node model then a multi-node model developed by connecting several nodes in series. Although the model showed accurate performance prediction for double glazed collector for a short term test, it is not suitable for variable flow rates.

Scnieders [1997] analyzed one stationary and five different dynamic models of solar collectors in different ways. The models were applied to a vacuum tube solar collector and the experimentally measured data were compared to the energy yield prediction. The collector was divided into several nodes in the flow direction to transfer the partial differential equations to an ordinary differential equations set. The most complicated model applied was a 3n-node-model; however the model was not suitable for variable flow rates. The study turned out that the stationary model overestimated the collector output in the case short time interval input, while the dynamic models yield similar results in the case of long time interval inputs.

Hilmer et al. [1999] presented a method to calculate the short-term dynamic behavior of unglazed solar collectors, working with varying fluid flow rate. With the assumption of steady-state heat transfer between the fluid and the absorber, the method showed good accuracy in the case of unglazed solar collectors presented by a simple two temperatures nodes model.

Zuefa and Magiera [2000] presented a mathematical model for heat transfer in a system involving a solar collector and a heat exchanger. In the proposed model the solar collector and the heat exchanger considered as a lumped parameter structure. The study enables an optimization to the system operation. The model validated experimentally

under steady-state conditions; assuming constant initial temperature, constant ambient temperature and a constant radiant energy density. With another assumption that these conditions are satisfied in a short time period.

Volker et al. [2002] published an experimental study conducted in a water flat-plate solar collector with laminar flow conditions to analyze the flow distribution through the collector. The flow distribution in relation to the overall discharge through the actual collector was experimentally determined. The loss coefficient for the pipe junctions in relation to the local Reynolds-number was investigated. The author noticed, the more uniform the flow distribution, the higher the collector efficiency. However uniform flow distributions are not always present in solar collectors.

Articles analyzing the possibilities of utilizing Artificial Neural Networks (ANN) to predict the operating parameters of flat-plate solar collector have been published. Farakas and Geczy-Vig [2003] introduced a different approach to the modeling of flat-plate solar collector. A sensitivity study was performed on the parameters of the neural network. The proposed ANN structures were trained and validated using Hottel-Vhillier model.

Kalogirou [2005] developed six ANN models for the prediction of standard performance collector equations coefficients, wind and no-wind conditions, the incident angle modifier coefficients at longitudinal and transverse directions, the collector time constant, the collector stagnation temperature and the collector capacity were considered. The study based on a steady-state operation conditions.

The thermal performance of flat-plate solar collector is strongly related to the flow distribution through the absorber tubes; Duffie and Beckmann [2006]. Some researchers studied the flow distribution parameter effect on the collector.

Fan et al. [2007] investigated experimentally and theoretically the flow and temperature distribution in a solar collector panel with an absorber consisting of horizontally inclined fins. Numerically, the flow and heat transfer in the collector panel were studied by the means of CFD calculations. Experimentally, the flow distribution through the absorber evaluated by means of temperature measurements on the backside of the absorber tubes. Their results showed a good agreement between the CFD results and the experimental data at high flow rates. However for small flow rates, large differences appeared between the computed and measured temperatures. This disagreement is most likely due to the oversimplification of the solar collector model.

Augustus and Kumar [2006] developed mathematical model to predict the thermal performance of an unglazed transpired collector, also known as perforated collector- a new development in the solar collector technology. Figure 2.2 illustrates this type of collectors. The model was based on the heat transfer expressions for the collector components, and empirical relations for estimating the various heat transfer coefficients. The authors analyzed the results of the model to predict the effects of key parameters on the performance of the collector. Their results showed that the solar absorptivity, collector pitch, and airflow rate have the strongest effect on collector heat exchange effectiveness as well as efficiency.

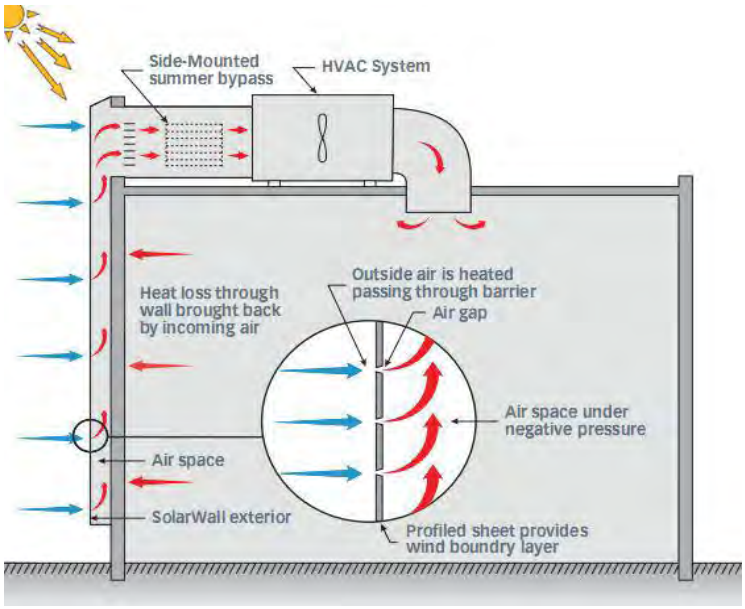

Figure 2.2: Perforated collector - Rooftop HVAC Unit
[www.SolarWall.com]

Molero et al. [2009] presented a 3-D numerical model for flat-plate solar collector considers the multidimensional and transient character of the problem. The effect of the non-uniform flow on the collector efficiency was quantified and the degree of deterioration of collector efficiency was defined. Their analysis showed that this deterioration increases with the increase of the flow non-uniformity, although this effect is very limited .The model was verified with a steady-state conditions. Their results shows that the collector efficiency does not change appreciably even when the flow at the outer risers is 1.5 times the flow of the central one but the outlet temperatures for each tube are very dissimilar.

Anderson et al. [2009] examined the performance of different colored solar collector. Based on the transmittance-absorptance product of different colored collectors the theoretical performances of these collectors were determined using the Hottel-

Whillier-Bliss 1-D steady-state model presented by Duffie and Beckmann [2006]. Their result showed that coloured solar collector absorbers can make noticeable contributions to heating loads, but the thermal efficiency was lower than highly developed selective coating absorbers.

Singh et al. [2009] calculated the overall heat loss coefficients of the trapezoidal cavity absorber for different types of pipes and covers concentrated collectors. The thermal performance of eight set of trapezoidal absorbers for linear concentrating collectors were analyzed and studied under constant flow rate and steady-state temperatures. Their analysis found that the heat loss coefficient increased with the absorber temperature, the double glass cover also reduced the overall heat loss coefficient by 10-15% compared to single glass cover.

Cadaflach [2009] has presented a detailed numerical model for flat-plate solar collector. He noticed that the heat transfer through the collector is essentially 1-D; some bi-dimensional and three-dimensional effects always occur due to the influence of the edges and the non-uniform effects, for example, there are temperature gradients in both the longitudinal and transversal directions. However, the main heat transfer flow remains one-dimensional. The model was an extension of the model of Duffie and Beckman [1991]. The model was verified by an experiment data of single and double glazed collectors under steady-state conditions.

Martinopoulos et al. [2010] developed a polymer solar collector in which the solar energy is directly absorbed by the black-colored working fluid. The model was investigated both experimentally and with computational fluid dynamics (CFD). As a validation of the CFD model, the obtained values for the temperature and velocity

distribution over the collector area using the CFD modeling were found to be in good agreement with the experimental results .The performance of the collector was obtained by CFD under steady-state conditions.

Zima and Dziewa [2011] presented a one dimensional mathematical model for simulating the transient processes which occur in liquid flat-plate solar collectors. The model considers the distributed parameters of the solar collector, the properties of the working fluid, air gap and absorber were computed in real time, the heat transfer coefficients were also computed in the on line mode. The presented model considers the time-dependent boundary conditions. The assumptions made for the proposed model were:

- All elements of the analyzed control volume have dimensions identical to the elements of the real collector.
- The operating fluid flows uniformly through all tubes.
- The properties of the glass cover and insulation are constants.
- All heat transfer coefficients computed in real time.

The experimental verification showed a satisfactory convergence of the measured and calculated fluid temperatures at the collector outlet. This study relay heavily on the model developed in Zima and Dziewa [2011]

In this study, the author will employ five nodes model that represent all the flat-plate solar collector's layers (cover, air-gap between cover and absorber, fluid flow, absorber and the insulation layer). The proposed model considers the distributed parameters of the collector. In the model the boundary conditions are taken to be time-dependent (sun radiation and ambient conditions). All the thermo-physical properties of

the fluid, absorber and air gap are computed in online mode (time-dependents). The method is based on solving the energy conservation equations for the glass, air gap, absorber, working fluid and insulation. The differential equations derived are solved using the implicit finite-difference method in an iterative scheme utilizing the MATLAB software. In order to verify the proposed code, measurements were carried out using an existing flat-plate solar collector. This study discusses the validation of the proposed method by comparing the predicted to the measured results.

CHAPTER 3 - THEORETICAL MODELING

The derivation of the mathematical model that portrays the operation of a flat-plate solar collector under transient conditions and the proposed method used to solve this model are presented in this chapter.

3.1. The Mathematical Model Development Of A Flat – Plate Solar Collector System

This section presents a mathematical model describing the flat-plate solar collector system considering the transient properties of its different zones. In the proposed model, the analyzed control volume of the flat-plate solar collector contains one tube that is divided into five nodes (glass cover, air gap, absorber, fluid and the insulation) perpendicular to the liquid flow direction, figure 3.1.

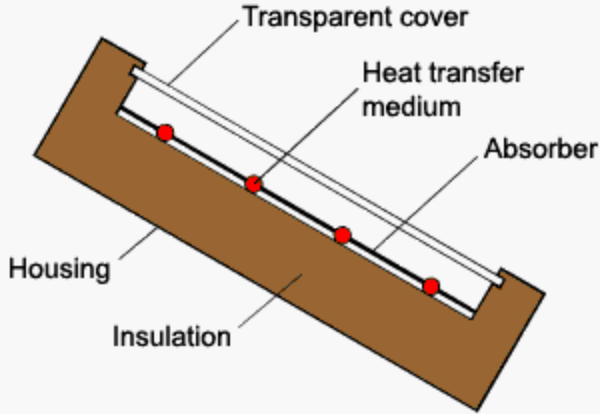

Figure 3.1: Sketch of the five nodes analyzed in the flat-plate solar collector model

The energy balance caused by the mass transfer during the circulating of the fluid within the solar collector is included by the definition that the collector's temperature depends on the coordinate in the direction of the fluid flow. Taking N nodes in the flow direction means that the model describes (5 x N) nodes. The governing equations were derived by applying the general energy balance for each zone in the analyzed control volume of the solar collector. For one-dimensional heat transfer, the general energy balance is given by:

$$\frac{dU}{dx} = \dot{Q}_{in} - \dot{Q}_{out} + \dot{Q}_v \tag{1}$$

where:

$\frac{dU}{dt}$ = the change in the internal energy.

$\dot{Q}_{in}$ = the heat transfer rate into the system.

$\dot{Q}_{out}$ = the heat transfer rate out of the system.

$\dot{Q}_v$ = the heat generation rate into the system.

To simplify the analysis of the solar collector, the following assumptions were made:

1. Uniform mass flow rate in the collector tubes.

$$\dot{m}_f = \frac{\dot{m}_t}{n} \tag{2}$$

where:

n = number of tubes in the solar collector

$\dot{m}_t$ = the total mass flow rate at the solar collector inlet

$\dot{m}_f$ = the mass flow rate in each tube

2. One-dimensional heat transfer through the system layers

3. There is no heat transfer in the direction of the flow, the energy transferred in the flow direction by mass transfer
4. The heat transfer from the collector edges is negligible
5. Properties of glass and insulation are independent of temperature (constant)
6. All thermo-physical properties of the fluid, air gap, and absorber are temperature dependent
7. The sky radiation and ambient conditions are time-dependents
8. Loss through front and back are to the same ambient temperature
9. The sky can be considered as a black body for long-wavelength radiation at an equivalent sky temperature
10. Dust and dirt on the collector are negligible

3.1.1 The glass cover

The small thickness of the cover makes it reasonable to consider a uniform temperature through it. And by considering constant properties of the glass, the governing equation can be derived from an energy balance in a differential volume of thickness δ_c and area of ($p\Delta z$). The heat transfers into the glass by convection between it and the ambient and by radiation from the sun and the absorber, figure 3.2.

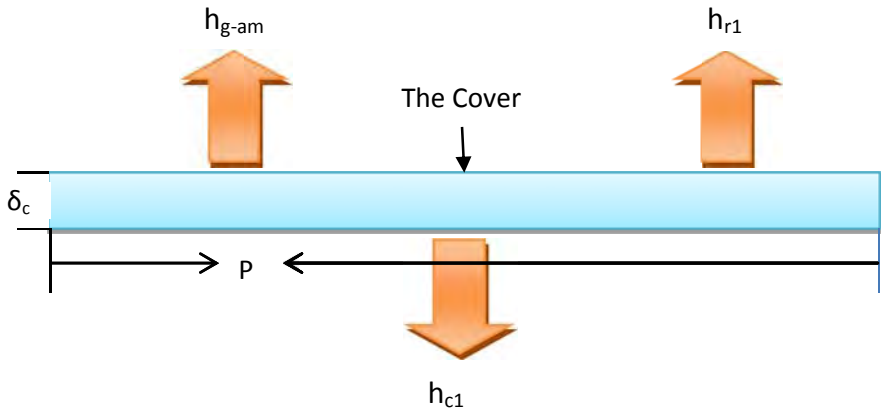

Figure 3.2: 1-D heat transfer in the cover

Then equation (1) can be written as:

$$c_g \rho_g V_g \frac{dT_g}{dt} = [h_{g.am}(T_{am} - T_g) + h_{r1}(T_{ab} - T_g) + h_{c1}(T_a - T_g) + \alpha G]p\Delta z \qquad (3)$$

where:

c = specific heat

ρ = density

V = volume

T = temperature

t = time

h = heat transfer coefficient

α = absorption coefficient

G = heat flux of solar radiation

p = tube pitch

Δz = spatial size of control volume

subscripts:

am = ambient
g = glass cover
a = air gap
ab = absorber
r = radiation
c = convection

3.1.2 The air gap between the cover and the absorber

By analyzing the air gap zone in the control volume of the solar collector, considering transient thermo-physical properties of the air, the heat transfers into the air gap by convection between it and the glass in upper side and the absorber in the other side figure 3.3.

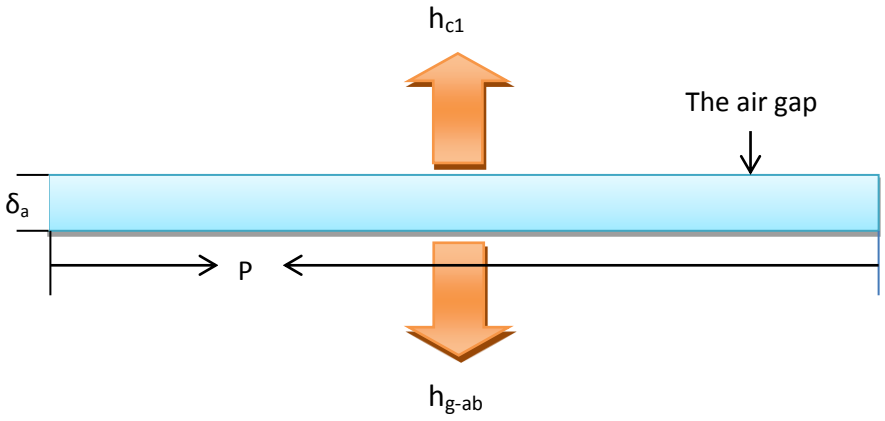

Figure 3.3: 1-D heat transfer in the air gap between cover and absorber

Then equation (1) can be written as:

$$c_a(T_a)\rho_a(T_a)\,V_a\frac{dT_a}{dt}=[h_{c1}(T_g-T_a)+h_{g.ab}(T_{ab}-T_a)]p\Delta z \qquad (4)$$

3.1.3 The absorber

Applying the heat energy balance for the absorber zone, figure 3.4, taking the transient thermo-physical properties of the absorber material and considering the solar irradiance on the absorber zone in the solar collector control volume, the radiation between the absorber and the glass cover, the conduction between the absorber and the insulation zone and the heat transfers by convection with the fluid flow, gives the following relation:

$$c_{ab}(T_{ab})\rho_{ab}(T_{ab})V_{ab}\frac{dT_{ab}}{dt} = [G(\tau\alpha) + h_{r1}(T_g - T_{ab}) + h_{c1}(T_a - T_{ab}) + \frac{k_i}{\delta_i}(T_i - T_{ab})]p\Delta z + \pi d_{in} h_f \Delta z (T_f - T_{ab}) \quad (5)$$

where:

($\eta\alpha$) = effective transmittance-absorption coefficient

k = thermal conductivity

δ = thickness

d = diameter

subscripts:

i = insulation

f = working fluid

in = inner

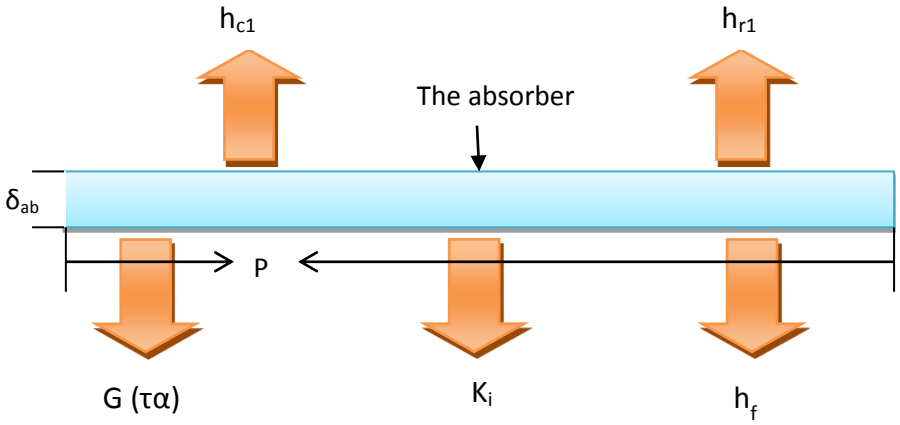

Figure 3.4: 1-D heat transfer in the absorber

3.1.4 The insulation

Analyzing the insulation zone in the solar collector control volume at constant properties for the insulation material and considering the conduction heat transfer between the insulation and the absorber with the radiation between the insulation and the surrounding ambient, figure 3.5.

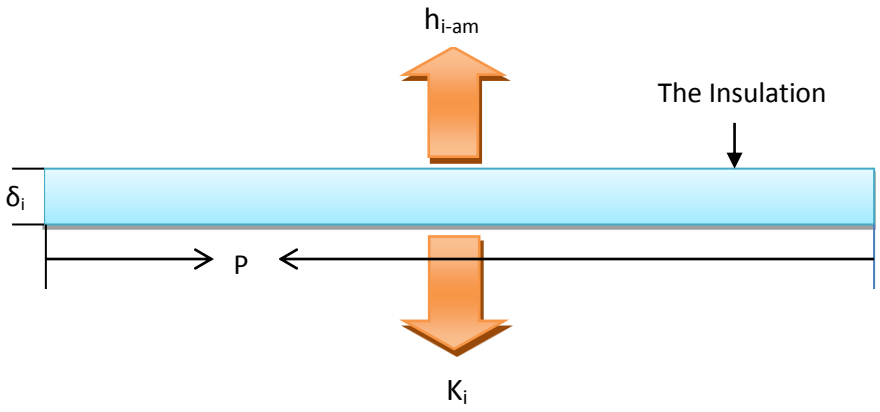

Figure 3.5: 1-D heat transfer in the insulation

The general heat energy balance equation (1) can be written as:

$$c_i \rho_i V_i \frac{dT_i}{dt} = \frac{k_i}{\delta_i}(T_{ab} - T_i) + h_{i\,am}(T_{am} - T_i) \tag{6}$$

3.1.5 The working fluid

Figure 3.7 shows the energy balance in a control volume of the working fluid in a flat-plate solar collector. Taking in consideration the change in total energy with time and the total heat transferred into the fluid control volume, the energy balance under transient properties of the working fluid can be written as:

$$c_f(T_f)\rho_f(T_f)A\frac{\partial T_f}{\partial t} = \pi d_{in} h_f (T_{ab} - T_f) - \dot{m}_f\, c_f(T_f)\frac{\partial T_f}{\partial z} \tag{7}$$

where:

A = the pipe cross sectional area

$\dot{m}$ = working fluid mass flow rate

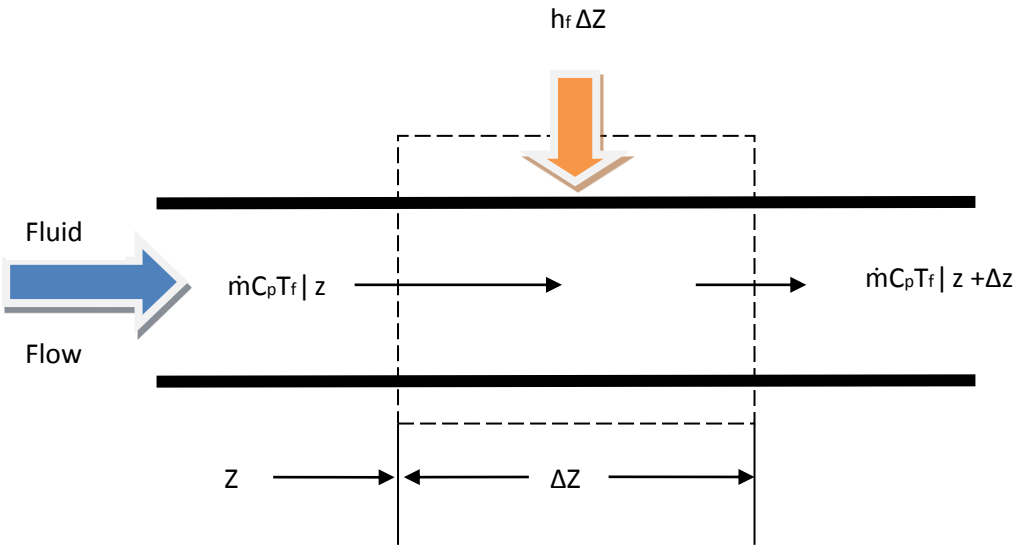

Figure 3.6: Energy balance in a control volume of the working fluid in flat-plate solar collector

At the fluid flow node simulation, ignoring the mass and momentum equations does not affect the validity of the proposed model and does not generate any errors on the computations. But generates such a model with a fewer equations and simpler form which make it faster so reach the numerical solution.

3.1.6 The storage tank

Figure 3.8 shows the conservation of energy in a control volume of the storage tank. Applying the first low of thermo dynamics over the tank control volume:

$$\frac{dE_{cv}}{dt} = \dot{Q} - \dot{W} + \dot{m}_{in}\left(h + \frac{V^2}{2} + gz\right) - \dot{m}_{out}\left(h + \frac{V^2}{2} + gz\right) \tag{8}$$

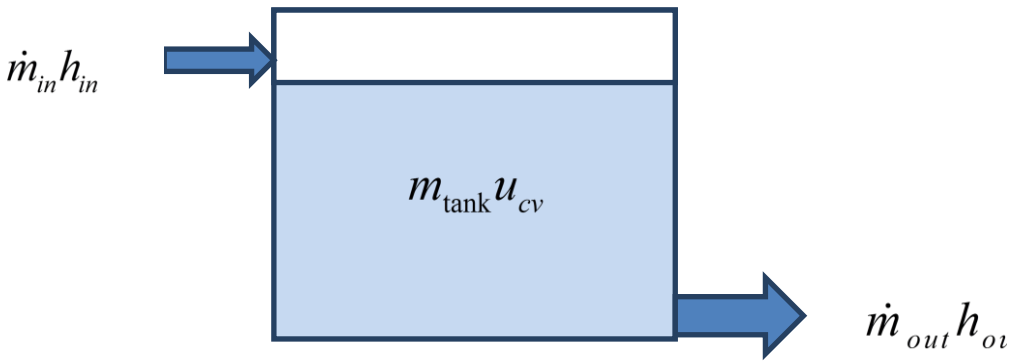

Figure 3.7: Storage tank control volume

In the tank case there is no work done in the system. Also, by neglecting the changes in the kinetic and potential energy, we can write approximate $e_{cv} = u_{cv}$ and $e_{flow} = h_{flow}$. With this approximation we can write:

$$\frac{d(mu)_{cv}}{dt} = \dot{Q}_{loss} + \dot{m}_{in}h_{in} - \dot{m}_{out}h_{out} \tag{9}$$

3.2 The Numerical Solution For The Solar Collector Mathematical Model

The partial differential equations system has been solved using the implicit finite difference method. The time and dimensional derivatives were replaced by a forward and a backward difference scheme, respectively as:

$$\frac{dT_m}{dt} = \frac{T_{m,j}^{t+\Delta t} - T_{m,j}^{t}}{\Delta t}$$
$$\frac{dT_f}{dz} = \frac{T_{f,j}^{t+\Delta t} - T_{f,j-1}^{t+\Delta t}}{\Delta z} \qquad (10)$$

where:

m = an index of values g, a, ab, f, and i

j = the node number in the flow direction (z)

The final formula of the equation system is:

$$T_{g,j}^{t+\Delta t} = \frac{1}{F_j \Delta t} T_{g,j}^{t} + \frac{B_j}{F_j} T_{am}^{t+\Delta t} + \frac{C_j}{F_j} T_{ab,j}^{t+\Delta t} + \frac{D_j}{F_j} T_{a,j}^{t+\Delta t} + \frac{E}{F_j} G^{t+\Delta t} \qquad (11)$$
$$j = 1, 2, .., N$$

$$T_{a,j}^{t+\Delta t} = \frac{1}{H_j \Delta t} T_{a,j}^{t} + \frac{G_j}{H_j} (T_{g,j}^{t+\Delta t} + T_{ab,j}^{t+\Delta t}) \qquad (12)$$
$$j = 1, ..., N$$

$$T_{ab,j}^{t+\Delta t} = \frac{1}{Q_j \Delta t} T_{ab,j}^{t} + \frac{K_j}{Q_j} G^{t+\Delta t} + \frac{L_j}{Q_j} T_{g,j}^{t+\Delta t} + \frac{M_j}{Q_j} T_{a,j}^{t+\Delta t} + \frac{O_j}{Q_j} T_{f,j}^{t+\Delta t} + \frac{P_j}{Q_j} T_{i,j}^{t+\Delta t} \qquad (13)$$
$$j = 1, 2, .., N$$

$$T_{f,j}^{t+\Delta t} = \frac{1}{U_j \Delta t} T_{f,j}^{t} + \frac{R_j}{U_j} T_{ab}^{t+\Delta t} + \frac{S_j}{U_j \Delta z} T_{f,j-1}^{t+\Delta t} \qquad (14)$$
$$j = 1, 2, .., N$$

$$T_{i,j}^{t+\Delta t} = \frac{1}{X_j \Delta t} T_{i,j}^{t} + \frac{V_j}{X_j} T_{ab}^{t+\Delta t} + \frac{W_j}{X_j} T_{am}^{t+\Delta t} \qquad (15)$$
$$j = 1, 2, .., N$$

$$T_{\text{tank}}^{t+\Delta t} = \frac{\dot{m}_{tot} c_p(t_f)}{m_{\text{tank}} c_v(t_f)} \Delta\tau (T_{f,n}^t - T_{\text{tank}}^t) - h_{\text{tank\_amb}} \frac{A_{\text{tank}}}{m_{\text{tank}} c_v(t_f)} \Delta\tau (T_{\text{tank}}^t + T_{am}^t) + T_{\text{tank}}^t \qquad (16)$$

where in the above equations

$$B_j = \frac{h_{g,am,j}}{c_g \rho_g \delta_g}, \quad \mathrm{C}_j = \frac{h_{r1,j}}{c_g \rho_g \delta_g}, \quad \mathrm{D}_j = \frac{h_{c1,j}}{c_g \rho_g \delta_g},$$

$$E = \frac{\alpha}{c_g \rho_g \delta_g}, \quad \mathrm{F}_j = \frac{1}{\Delta t} + B_j + \mathrm{C}_j + D_j,$$

$$J_j = c_{ab}(T_{ab})_j \rho_{ab}(T_{ab})_j [p\delta_{ab} + \pi(r_{out}^2 - r_{in}^2)],$$

$$K_j = \frac{p(\tau\alpha)}{J_j}, \quad \mathrm{L}_j = \frac{h_{r1,j} p}{J_j}, \quad \mathrm{M}_j = \frac{h_{c1,j} p}{J_j},$$

$$O_j = \frac{\pi d_{in} h_{f,j}}{J_j}, \quad \mathrm{P}_j = \frac{p k_i}{J_j \delta_j},$$

$$G_j = \frac{h_{c1,j} p}{c_a(T_a)_j \rho_a(T_a)_j (p\delta_{ab} + \pi r_{out}^2)}, \quad H_j = \frac{1}{\Delta t} + 2G_j,$$

$$Q_j = \frac{1}{\Delta t} + L_j + M_j + O_j + P_j,$$

$$R_j = \frac{\pi d_{in} h_{f,j}}{c_f(T_f)_j \rho_f(T_f)_j A}, \quad S_j = \frac{\dot{m}_f}{\rho_f(T_f)_j A},$$

$$U_j = \frac{1}{\Delta t} + R_j + \frac{S_j}{\Delta z}, \quad \mathrm{V} = \frac{2k_i}{c_i \rho_i \delta_i^2}, \qquad (17)$$

$$W_j = \frac{2h_{i,am,j}}{c_i \rho_i \delta_i} \quad \text{and} \quad X_j = \frac{1}{\Delta t} + V + W_j$$

:

In the proposed method all the temperatures have to meet the following error criteria in order to stop the iteration process:

$$\left| \frac{T_{j,(k+1)}^{t+\Delta t} - T_{j,(k)}^{t+\Delta t}}{T_{j,(k+1)}^{t+\Delta t}} \right| \le \vartheta \qquad (18)$$

where

T = is the evaluated temperature in node j

ϑ = is an acceptable tolerance of iteration (e.g. 10^{-4})

k = 1, 2… is the iteration counter for every single time step

In addition to the iteration stop condition, the whole process as all should satisfy the following condition – the Courant-Friedriches-Lewy stability condition over each time step:

$$|\psi| \le 1, \quad \psi = \frac{\omega_f \Delta t}{\Delta z} \tag{19}$$

By satisfying this condition the numerical solution is reached with a speed Δz / Δt, greater than the physical speed ω_f.

3.3 The Heat Transfer Correlations

In the proposed solution method the heat transfer coefficients were calculated using the following formulas

- The radiation between the absorber and glass cover, Duffie and Beckmann [2006].

$$h_{r1,j} = \frac{\sigma(T_{ab,j}^2 + T_{g,j}^2)(T_{ab,j} + T_{g,j})}{(1/\varepsilon_{ab}) + (1/\varepsilon_g) - 1} \tag{20}$$

where

h = heat transfer coefficient

ζ = Stefan-Boltzmann constant

ε = the emissivity

- The free convection in the inclined air gap.

$$h_{c1,j} = \frac{Nu_{a,j} k_{a,j}}{\delta_a} \tag{21}$$

while the Nusselt number calculated using the formula giving by Hollands [1976].

$$Nu_{a,j} = 1 + 1.44\left[1 - \frac{1708[\sin(1.8\beta)]^{1.6}}{Ra_j \cos(\beta)}\right] * \left(1 - \frac{1708}{Ra_j \cos(\beta)}\right)^{+} + \left[\left(\frac{Ra_j \cos(\beta)}{5830}\right)^{1/3} - 1\right]^{+}$$

with (22)

$$Ra = \frac{g\beta\Delta T L^3}{\nu\alpha}$$

where:

Ra = Rayleigh number

β = the thermal expansion coefficient

L = the length of the pipe

ν = the kinematic viscosity

α = the thermal diffusivity

In the above formula, the segments denoted by „+' shall be considered only they assume positive values. Otherwise they shall be replaced by zero value.

- Convection on the external surface of the cover and insulation, Duffie and Beckmann [2006].

$$h_{c2} = \frac{Nu_{am} k_{am}}{\delta} \tag{23}$$

Taking

$$Nu_{am} = .86\,\mathrm{Re}_{am}^{1/2}\,\mathrm{Pr}_{am}^{1/3} \quad \text{and} \quad \delta = \frac{4ab}{\sqrt{a^2 + b^2}} \tag{24}$$

where

Re = Reynolds number
Pr = Prandtl number

where a and b are length and width of the collector, respectively, in meters.

- The equivalent heat transfer coefficient on the external surface of the glass

$$h_{g,am,j} = \frac{\sigma \varepsilon_g (T_{g,j}^4 - T_{sky}^4)}{T_{g,j} - T_{am}} + h_{c2} \tag{25}$$

The sky temperature calculated using Swinbank's formula

$$T_{ky} = .0552\ T_{am}^{1.5} \tag{26}$$

- The equivalent heat transfer coefficient on the external surface of the insulation

$$h_{i,am,j} = \frac{\sigma \varepsilon_i (T_{i,j}^4 - T_{sky}^4)}{T_{i,j} - T_{am}} + h_{c2} \tag{27}$$

- Heat transfer on the internal surface of the collector tube.

$$h_{f,j} = \frac{Nu_{f,j} k_{f,j}}{d_{in}} \tag{28}$$

Where the Nusselt number calculated using the empirical Heaton formula suggested by Duffie and Beckman [2006]

$$Nu_{f,j} = Nu_{\infty} + \frac{a(\mathrm{Re}_{f,j}\,\mathrm{Pr}_{f,j}(d_{in}/L))^m}{1 + b(\mathrm{Re}_{f,j}\,\mathrm{Pr}_{f,j}(d_{in}/L))^n}; \quad 1 < \mathrm{Re}_{f,j}\,\mathrm{Pr}_{f,j}\frac{d_{in}}{L} \le 1000 \tag{29}$$

with the assumption that the flow inside of tubes is fully developed , the values of Nu_{∞}, a, b, m, and n are 4.4, 0.00398, 0.0114, 1.66, and 1.12, respectively, for the constant heat flux boundary condition.

CHAPTER 4- MATHEMATICAL MODEL PROGRAMING

Figure 4.1 shows a detailed flowchart entailing the various steps to solve the mathematical model developed in the previous chapter. This model is used for a flat-plate solar collector with single glass cover working in parallel channel arrangement model. All physical dimensions of the collector can be entered as inputs, which make it suitable to any single glass cover flat-plate solar collector without any modifications; however, the use of a second glass cover requires additional formula to be derived in order to determine the temperature histories of the second cover and of the medium between the covers.

As all the boundary conditions in the proposed model taken to be time dependent, the inputs data for the numerical code are the following measured data:

- Total fluid mass flow rate.
- Total flux of solar radiation.
- Ambient temperature.
- The initial fluid temperature in tank.

The software package used to code the model is MATLAB version R2011a. MATLAB is a programming package that can be used for algorithm development, data analysis, visualization, and numerical computation. The software is faster than traditional

programming languages including C, C++, and FORTRAN. The detailed MATLAB code developed for the model is presented in Appendix A.

The MATLAB code numerically solves the derived model and computes the transient temperature distributions for any cross-section at the collector beginning at time (t = 0), that is from the onset of the process till the total time of calculations that entered by user.

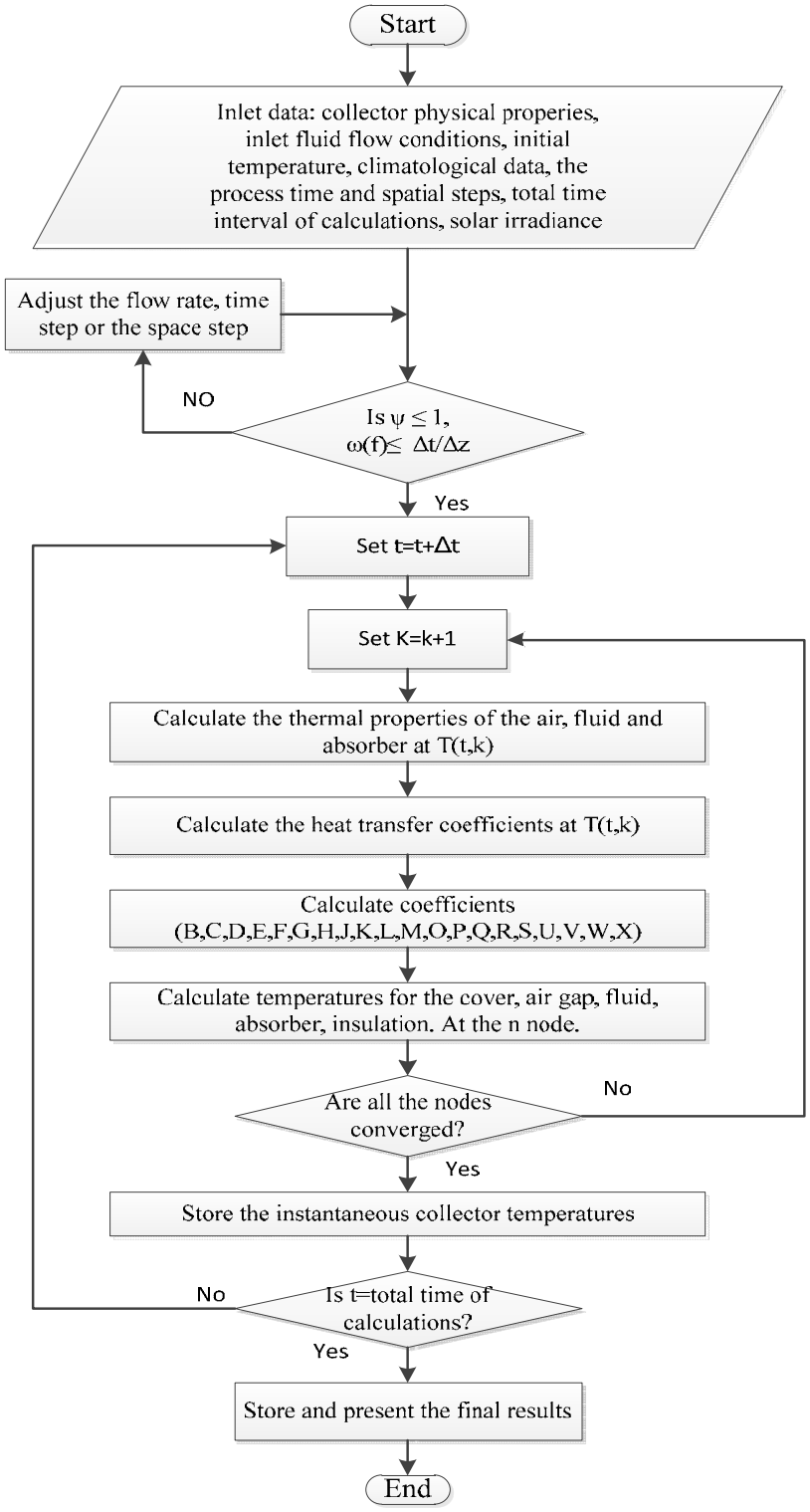

4. 1: MATLAB code flowchart

CHAPTER 5- DESIGN OF EXPERIMENT

All the experimental work that was done to verify the code took place in the Engineering department of Indiana University - Purdue University Fort Wayne, using an existing flat-plate solar collector.

The existing solar collector has one (80” x 39”) single glass cover SunMaxx flat-plate provided by Silicon Solar Inc. The plate consists of 8 tubes and 2 headers made of Copper with tube spacing of 5 inches and a diameter of 0.375 inches. While the absorber made of Red Copper with a black chrome selective surface, the flat-plate has 2 inches Rock Wool insulation, and cased by a frame of Aluminum. The SunMaxx flat-plate solar collector was mounted on a wooden frame at 45 degree angle. Figures 5.1 and 5.2 show a front and side view of the utilized solar collector, respectively.

Figure 5.1: Front view of the utilized solar collector

Figure 5.2: side view of the utilized solar collector

To circulate the water into the system, a Shurflo diaphragm pump (12 V DC, 1/12 horsepower, rated at 3 GPM) from MSC Industrial Supply Co. was used as shown in Figure 5.3. An on-off switch and inline fuse are mounted next to the flow meter on the solar collector's frame as shown in figure 5.4.

Figure 5.3: Water pump installation

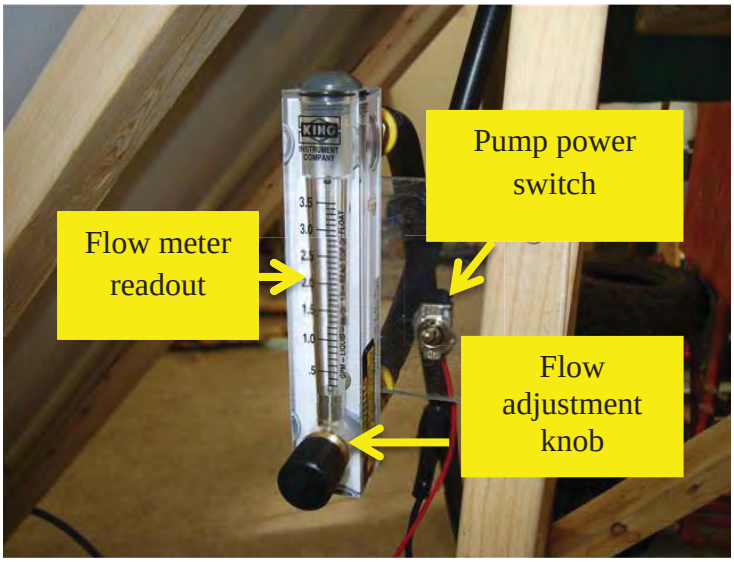

Figure 5.4: Flow meter and the pump power switch

Type K thermocouple was added to the existing setup in the inlet and outlet of the solar collector and another in the tank. The thermocouple at the inlet was placed in the flow stream after the pump, and the thermocouple at the outlet was placed in the flow stream just before the tank, as shown in figure 5.5.

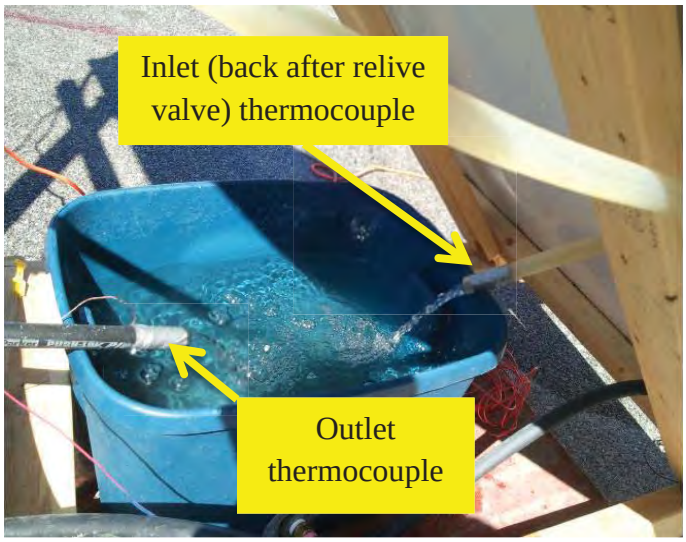

Figure 5.5: The inlet and outlet thermocouples locations

To read out and record the temperatures during the experiment, the HH1384 data logger 4-input thermometer model from Omega Engineering, Inc., figure 5.6, was used. This instrument is a digital, 4-input thermometer and data logger that accepts any K, J, E, T, R, S, N, L, U, B and C Type thermocouple temperature sensors. Powered by 6 “AA” batteries or DC 9V AC adaptor, comes with an USB interface with Windows Software, memory and read function (99 Sets) and 512 KB auto data logging capacity with adjustable logging interval.

Figure 5.6: HH1384 data logger 4-input thermometer

In order to calculate the input energy to the system the SDL-1 Solar Data Logger model from Micro Circuit Labs Co. was selected to measure the sun's irradiance at regular time intervals, figure 5.7. Its USB interface allowed the data to be loaded to the computer. The communications program Hyper Terminal was used to capture logged data to a text file to be analyzed and plotted using a spreadsheet program. The SDL-1 also reports the cumulative incident solar energy that it receives during deployment.

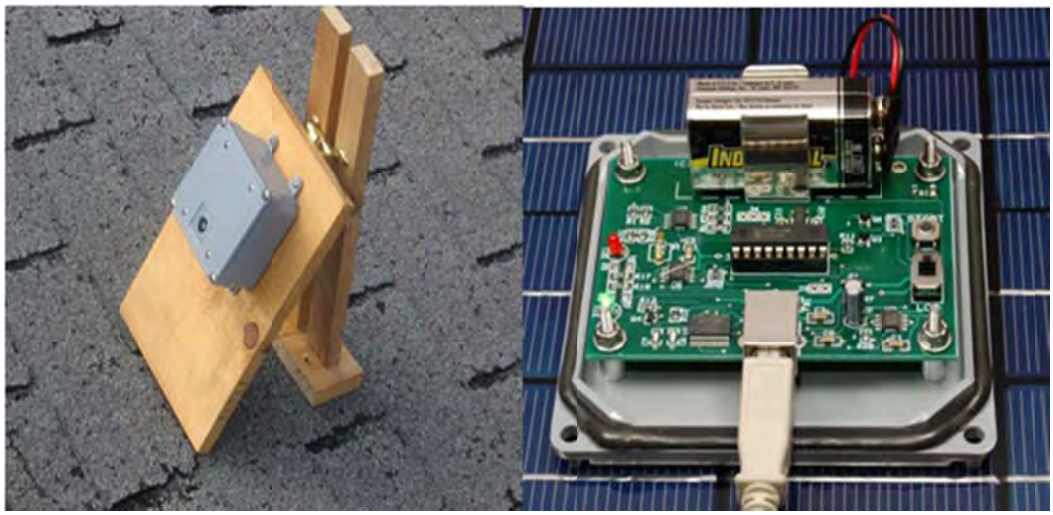

Figure 5.7: SDL-1 solar irradiance data logger

Several experiments were done on the solar collector. The first set of experiments was performed to verify the results obtained by running the code with a constant ambient temperature and a step function behavior for the solar radiation. These conditions satisfied by starting the solar collector from a uniform temperature and place under the sun radiation for an hour then moving it inside the lab (solar irradiance =0). This experiment procedure was repeated for three different flow rates.

The other set of experiments was basically to study the behavior of the solar collector by simply place it outside the Lab and run it for various time periods and flow rates in several days.

The data recorded during all the experiments was the inlet, outlet, tank and ambient temperatures along with the solar irradiance during the process. The temperatures were recorded every one minute interval, while the solar irradiance was an average of every 15 minutes interval.

CHAPTER 6- RESULTS AND DISCUSSION

This chapter presents the results obtained from the theoretical and experimental works. The first part of the analysis was a convergence study for the proposed numerical code. The second part presents a comparison between the numerical obtained temperature histories and the experimentally measured data. The following sections present the details of each section.

6.1 Convergence Study

The temperatures distributions obtained by the MATLAB code have been tested for different numbers of nodes (n= 4, 6, 8, 12, 24, 48, and 72) along the flow direction. Figure 6.1 shows the collector's outlet temperature obtained numerically for each number of nodes at constant flow rate ($\dot{V}$=1.5 GPM). In order to show the convergence of the proposed method in more details, a selected period of time from figure 6.1 includes the critical area of the curves (i.e., the solar irradiance step-change) is presented in figure 6.2.

As can be clearly seen from the figure, the proposed method converges when the number of nodes is 12 nodes. Table 6.1 present the running time and the range of error in the obtained temperatures compared to the 72 nodes model. However, the results suggest limit the number of nodes to 24 in order to optimize the cost of running time with acceptable differences from the optimum case of 72 nodes. Therefore, the case of 24 nodes represents the minimum bound of number of nodes for the convergence results.

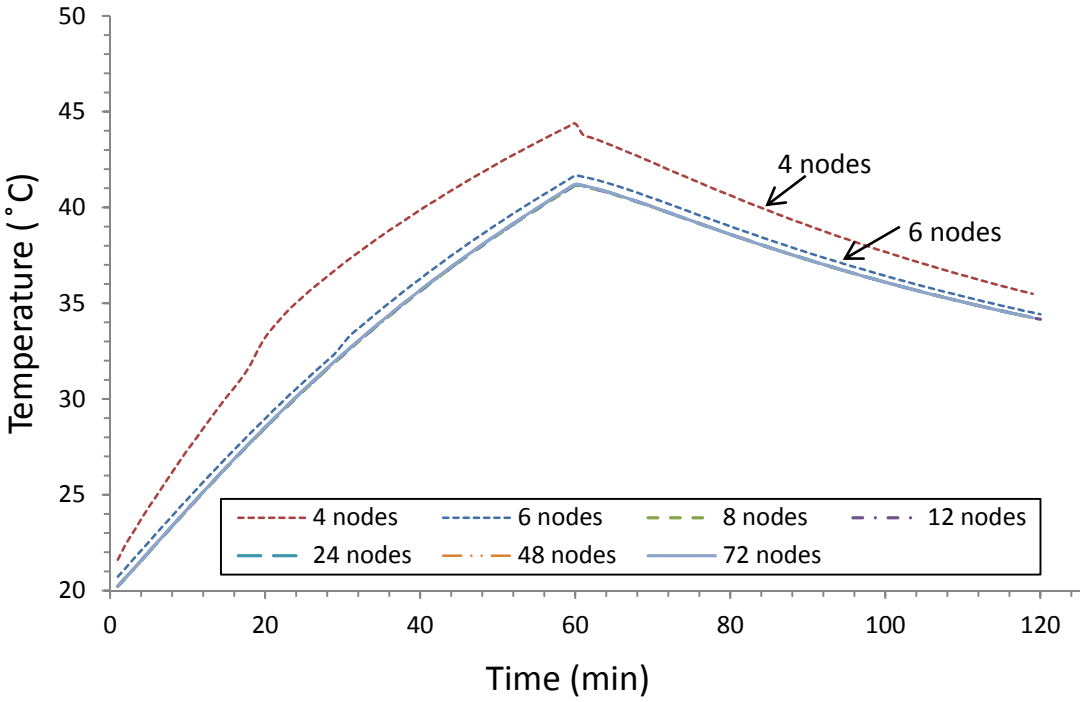

Figure 6.1: Outlet temperature histories for different number of nodes at 1.5 GPM

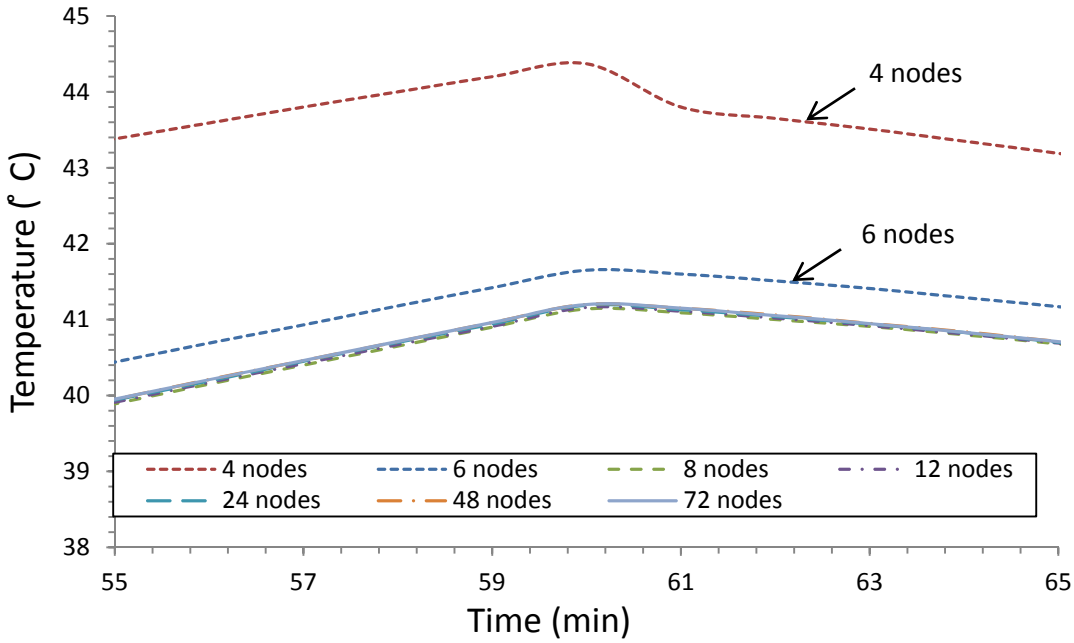

Figure 6.2: Selected period for the outlet temperature histories obtained for each number of nodes

Table 6.1: The range of error comparing to the 72 nodes model, and the running time of each number of nodes at 1.5 GPM

	Number of nodes (n)						
	4	6	8	12	24	48	72
Time-step (sec)	3.8	2.3	1.6	1.0	0.5	0.24	0.16
Range of error (˚C)	± 0.64	± 0.64	± 0.06	± 0.05	± 0.02	± 0.01	± 0
Running time (sec)	26.35	33.30	53.18	80.25	194.5	502.4	924

In order to analyze the response of the code to the transient inputs; the solar irradiance was represented by a two different step functions. The first one changes the irradiance magnitude after one hour while the second case it changes after 30 minutes. Figure 6.3 shows the output temperature of the working fluid predicted by the model for each case. The two cases ran for 24 nodes under the same conditions except for the solar radiation step function.

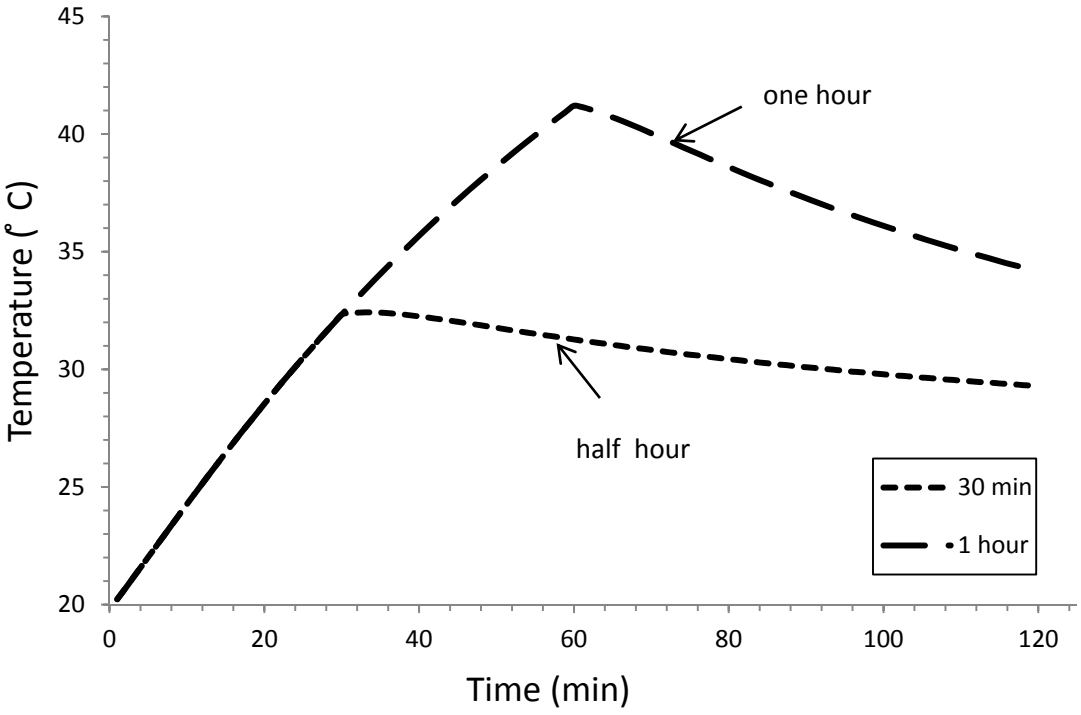

Figure 6.3: Outlet temperature for different input solar radiation

As was discussed in chapter 3, in order for the iteration process to converge the time step has to satisfy the Courant-Friedichs-Lewy stability condition. Figure 6.4 shows the numerically predicted histories of the fluid temperature at the collector's outlet that obtained by the MATLAB code, for three different time steps: 0.1 seconds, 0.5 second (the maximum time step satisfies the stability condition at 1.5 GPM and 24 nodes), and 2.0 seconds.

The lowest time step of 0.1 sec has resulted in more stability among all other time steps as shown in figure 6.4. However, it had a high running time cost. While the highest time-step of 2.0 seconds result has the shortest running time, it had a very poor stability. The best choice in this analysis is to use the highest time-step satisfies the Courant-Friedichs-Lewy stability condition (0.5 in this case), because it gives a very close results

to the 0.1 seconds case in an acceptable time coast. Table 6.2 presents the range of errors (compared to the 0.1 sec case) and the running cost for each case.

Table 6.2: The range of error compared to the 0.1 seconds case, and the running time for the same number of nodes running at different time steps.

	Time step Δt (seconds)		
	0.1	0.5	2.0
Range of error (˚C)	0	± 0.01	± 2.56
Running time (sec)	2355.0	194.5	47.0

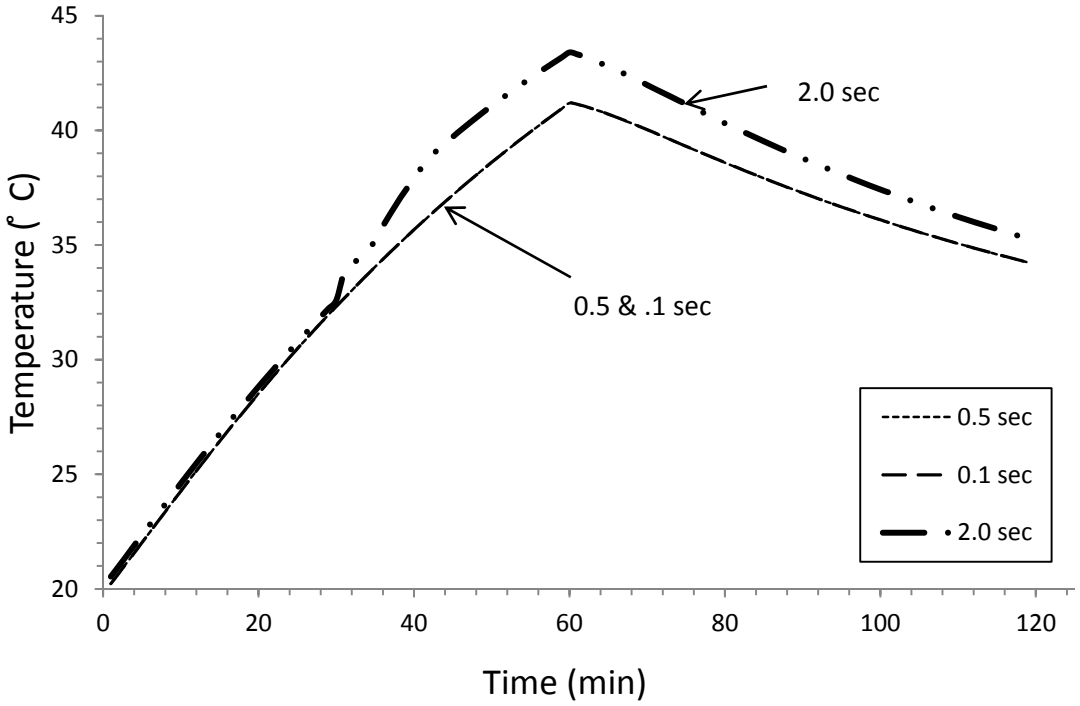

Figure 6.4: Outlet temperature histories obtained by 24 nodes at different time-steps.

The temperature history at the collector outlet was computed for four different flow rates (0.5, 1.0, 1.5, and 2.0 GPM) for the same number of nodes (48 nodes) and constant time step (0.1 second). Figure 6.5 shows the effect of the flow rate on the

working fluid outlet temperature. It can be easily seen how decreasing the flow rate results in more increase in the outlet temperature of the collector.

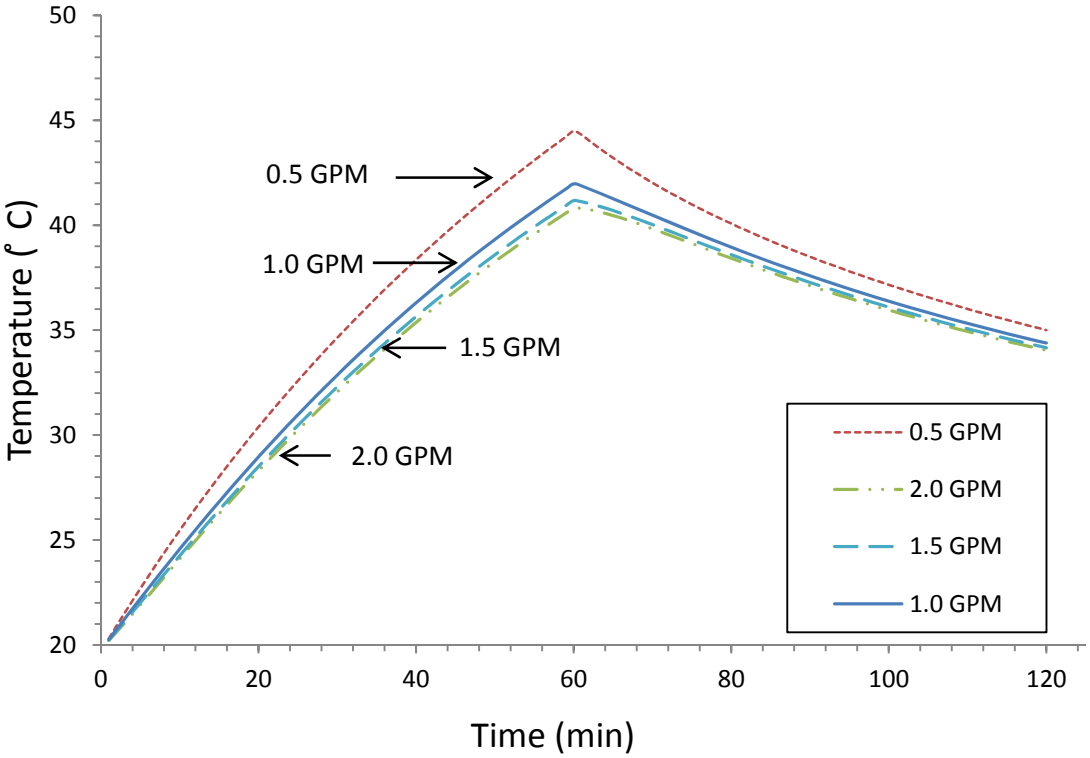

Figure 6.5: The temperature histories at the collector's outlet for different flow rates

The predicted temperature histories for particular elements of the collector including the cover, air gap, absorber, working fluid and insulation at selected cross-section node number 12 (L=0.95 m), are presented in figure 6.6. The results were obtained at 1.5 GPM and 24 nodes with the maximum stable time-step (0.5 seconds). Similar curve for the last node 24 is shown in figure 6.7. Such histories can be shown for each of the 48 analyzed cross-sections.

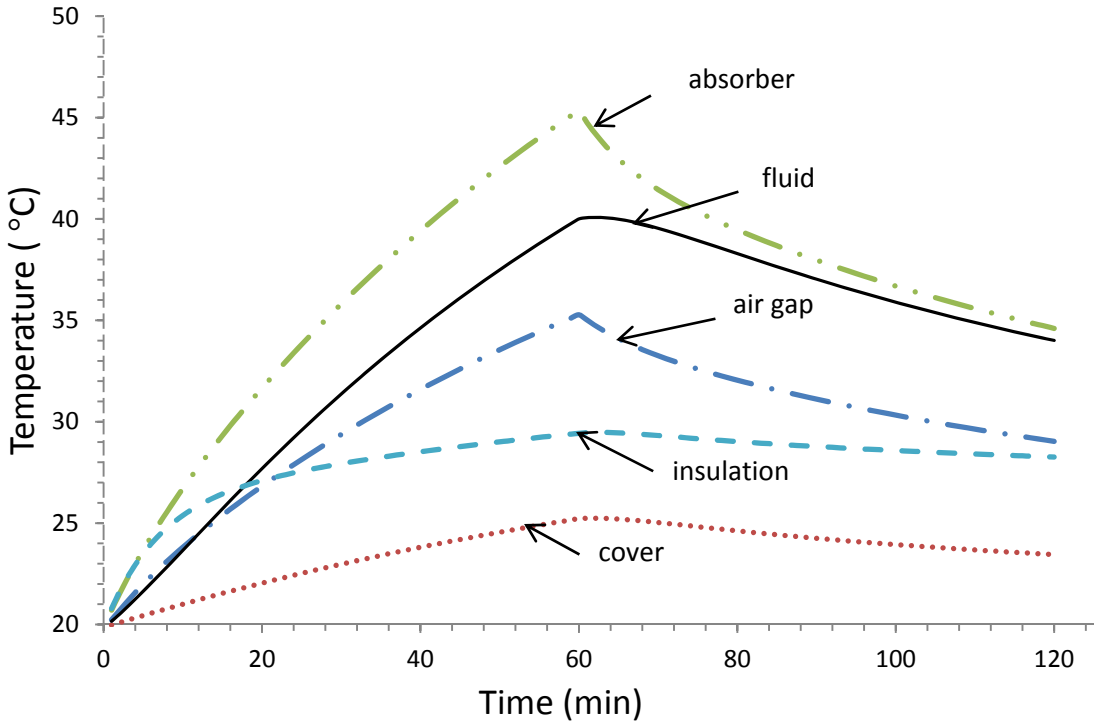

Figure 6.6: Temperature histories for all the analyzed cross section (node 12)

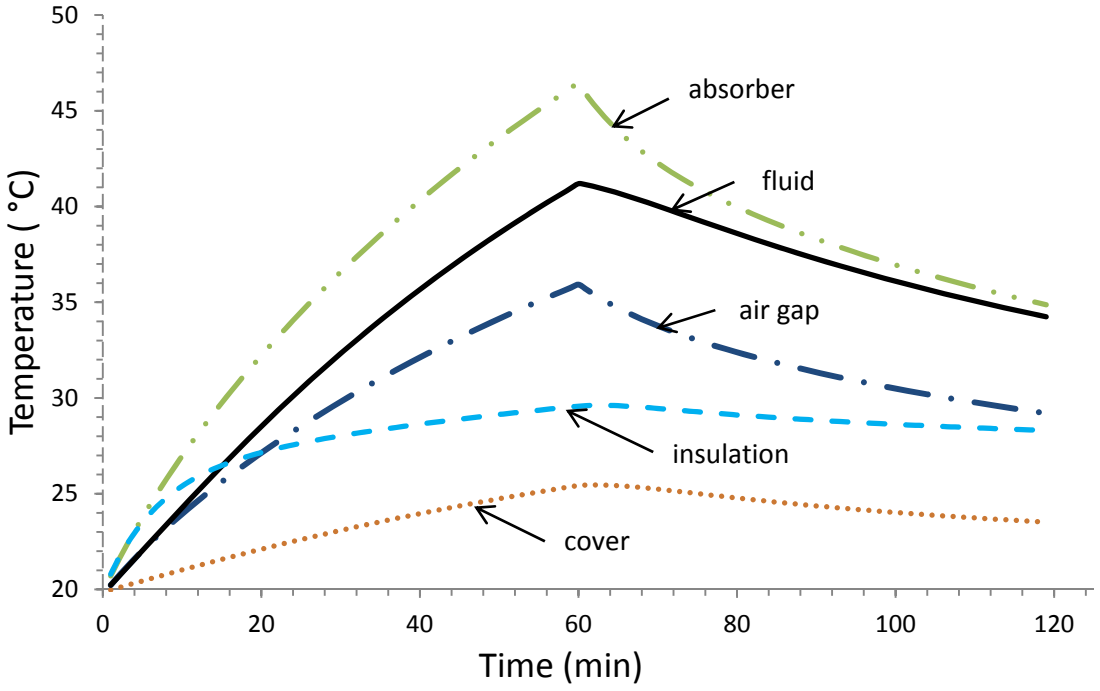

Figure 6.7: Temperature histories for all the analyzed cross section (node 24)

As it was expected the temperature of the absorber records the highest value along the running time, since the primary function of the absorber plate is to absorb as much as possible of the radiation reaching through the glazing, to lose as little heat as possible upward to the atmosphere and downward through the back of the container, and to transfer the retained heat to the circulating fluid. The high conductivity of the absorber resulted in the fast response of the working fluid's temperature to the change in in the absorber's temperature.

Also it can be seen how the insulation temperature changes very slowly, that is due to the low heat conductivity of the insulation material selected which is required to reduce the heat losses from the system.

The purpose of the cover is to admit as much solar radiation as possible and to reduce the upward loss of heat to the lowest attainable value. The glass cover material (patterned low-iron glass) used has a very high transmissivity with a small absorption coefficient. From the cover temperature history presented above the cover has the lowest variation along time, thus it works efficiently for this purpose.

The variation of the air gap zone temperature due to the convection and radiation heat transferred from the absorber, this loss can be reduced by evacuating the collector from air.

Figure 6.8 shows the predicted temperature histories of the solar collector at the inlet, outlet and the mid-point along the flow direction (node 12), the presented data were obtained using 24 nodes, 1.5 GPM.

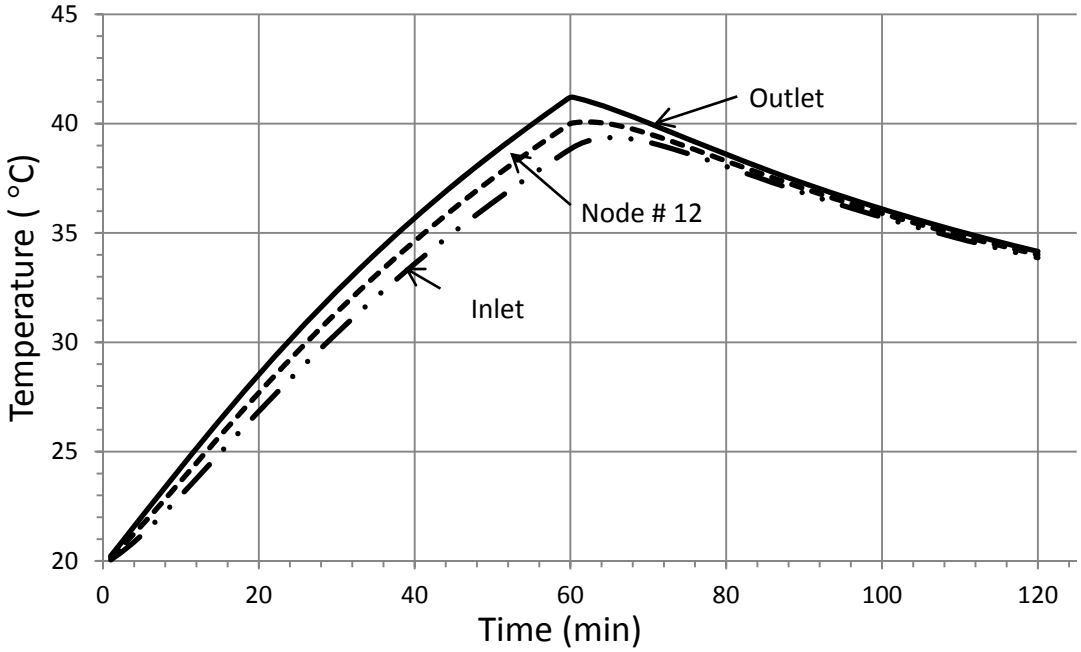

Figure 6.8: Working fluid temperature histories at the inlet, mid-point and the outlet

6.2 Experimental Verification

Several experiments were conducted in the months of March and April 2012 to verify the numerical model. The selected cases represent two different weather conditions. The weather data pertain to the experimental days are shown in table 6.1. All the experiments were conducted in the solar collector bench at the laboratory facilities of the engineering department in Indiana University Purdue University Fort Wayne with same procedure described in chapter 5.

Table 6.3: The weather details of the experimental dates

Day	Max ambient temperature ˚C	Min ambient temperature ˚C	Average wind speed (MPH)	weather
March 22	31	12	2	Sunny
March 29	20	4	3	Mostly cloudy

6.2.1 Case 1

The first case was selected on March 22, 2012 because it was a relatively warm day with a maximum temperature of 31˚C an average wind speed of 2.0 mph. The flow rate in the collector was adjusted at 1.5 GPM, the solar collector was placed outside the lab under the sun radiation for one hour, and then it was entered inside the lab. The inlet, outlet temperatures were measured and recorded every one minute. While the value of the solar irradiance was recorded as an average over 15 minutes intervals, the ambient temperature was with an average of 28˚C during the run with a small variation. Figures 6.9 and 6.10 present the temperature histories recorded and the average solar irradiance values during the experiment.

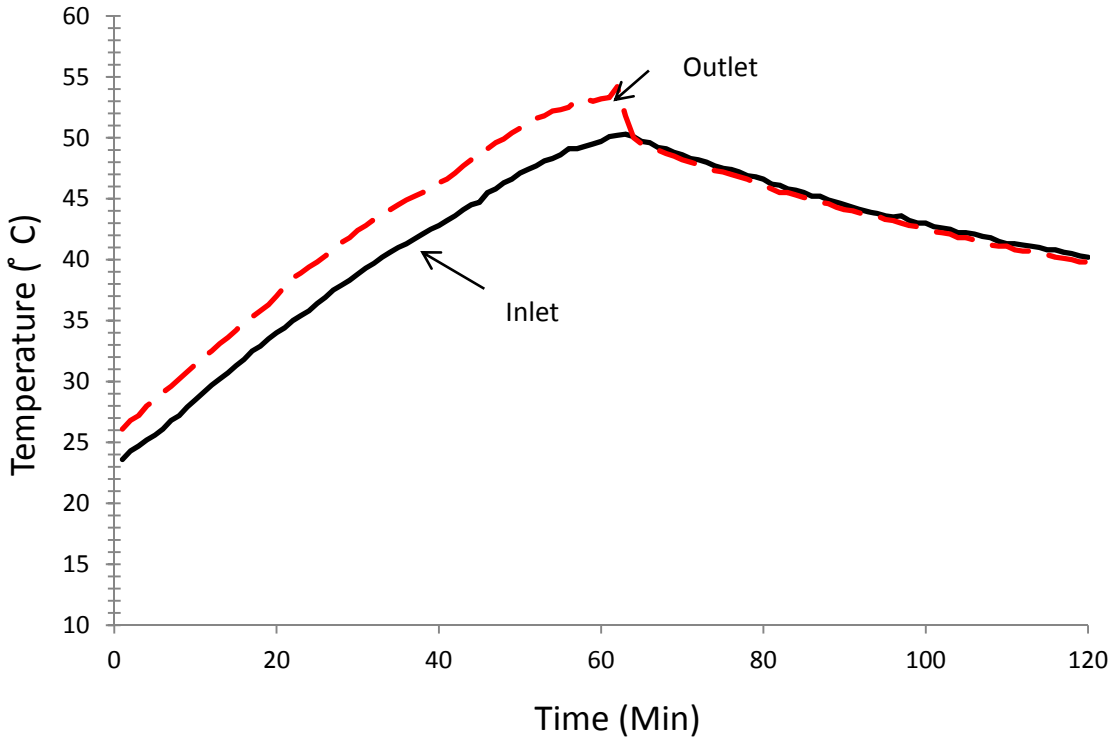

Figure 6.9: Recorded outlet, inlet temperature histories on March 22nd

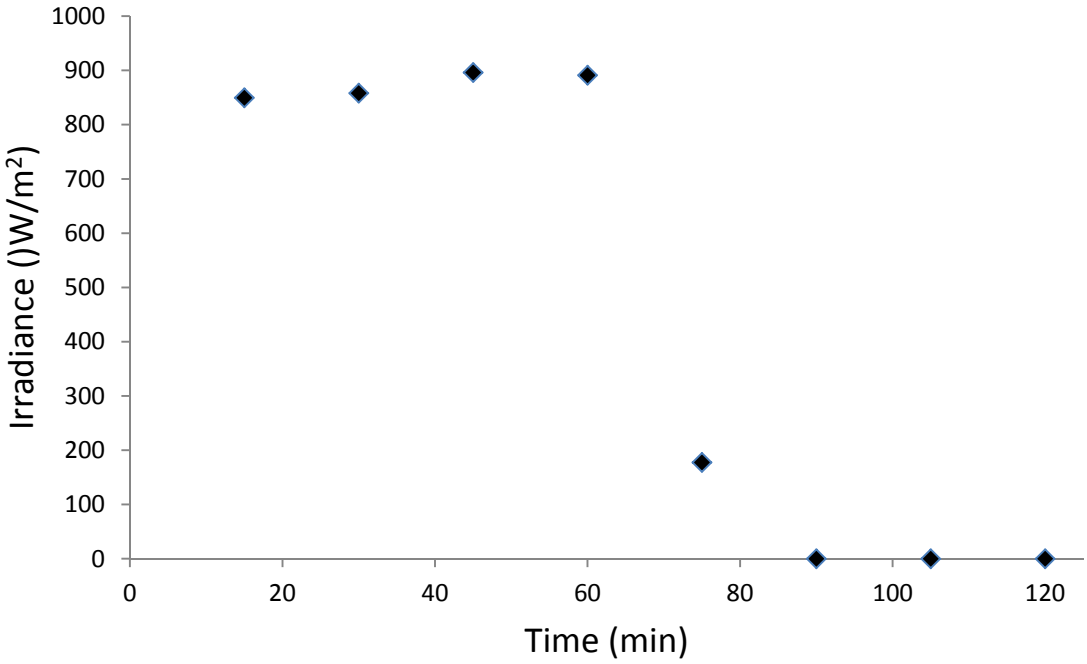

Figure 6.10: History of the recorded solar radiation on March 22nd

Figure 6.11 compares the measured temperature histories at the inlet and outlet nodes collected on March 22nd to the values predicted using the proposed numerical model. The comparison shows good agreement between measured and the predicted results. The maximum error was 3.6% for the inlet temperature, and 4.1% for the outlet temperature. The measured data is presented in Appendix B

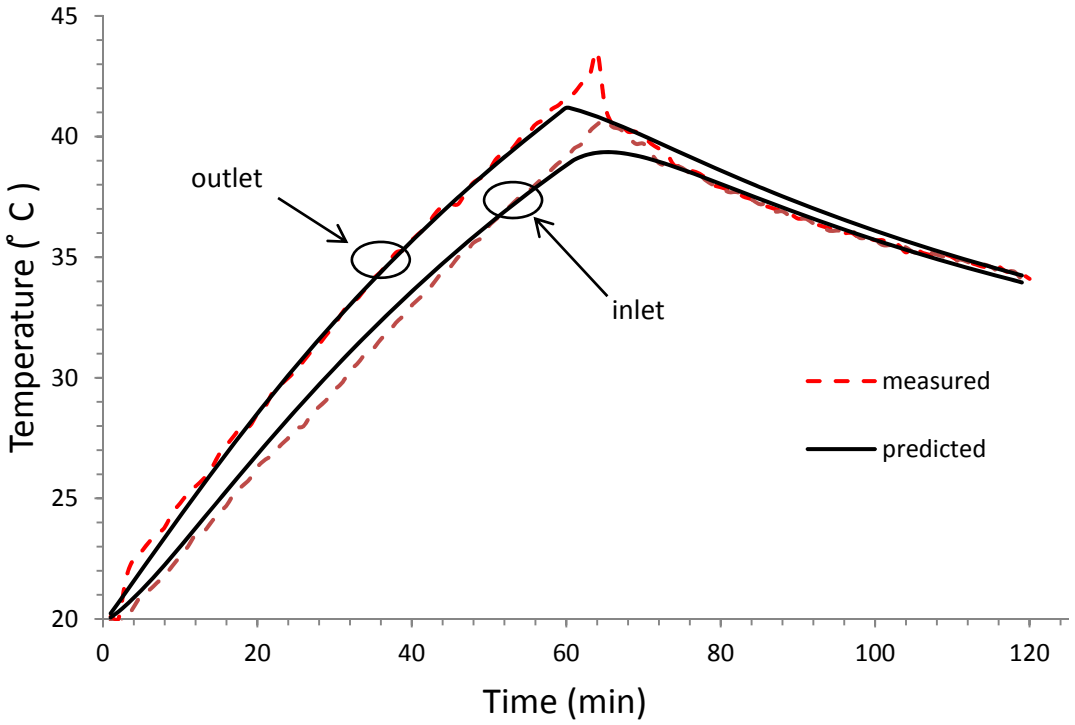

Figure 6.11: Comparison of measured and computed fluid temperatures histories at the solar collector inlet and outlet March 22nd

6.2.2 Case 2

The second selected case was March 29, 2012 has the least amount of sunshine and was mostly cloudy with a maximum temperature of 20˚C and an average wind speed of 3.0 mph. The flow rate in the collector was adjusted at 2.0 GPM, the solar collector was placed outside the lab under the sun radiation for an hour, and then it was entered inside the lab. The inlet, outlet temperatures were recorded every one minute, while the value of the solar irradiance was recorded as an average over 15 minutes intervals. The ambient temperature was with an average of 18˚C during the run with a small variation. Figures 6.12 and 6.13 present the temperature histories recorded and the average solar irradiance values during the experiment.

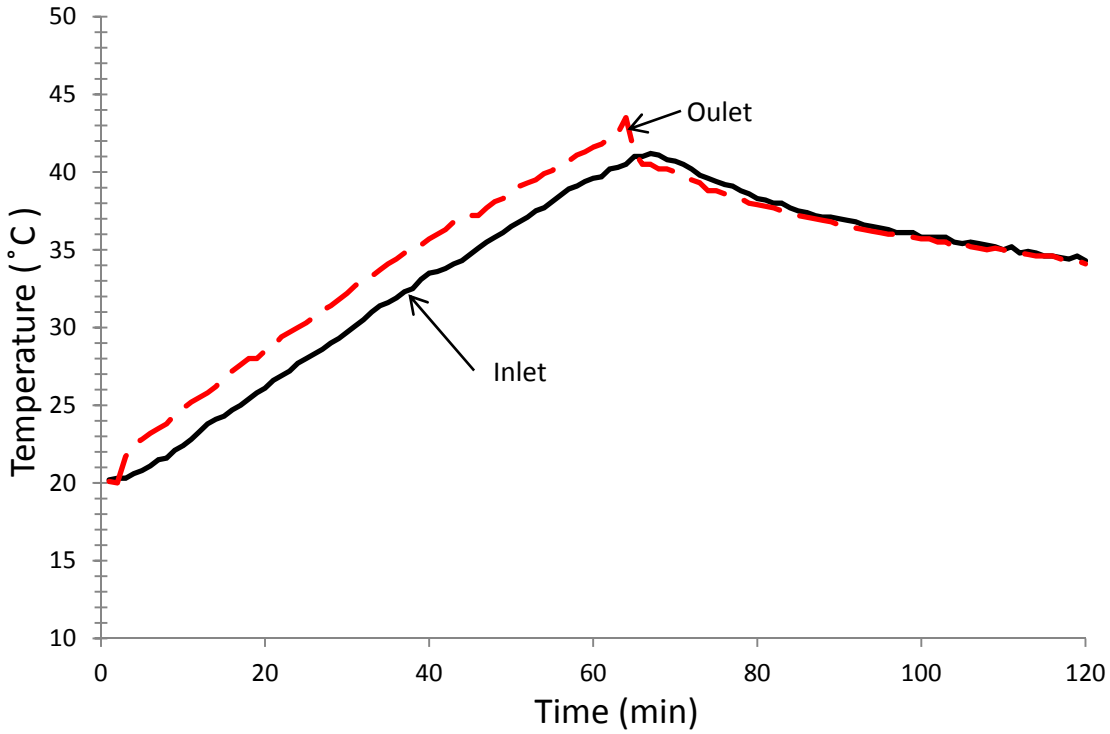

Figure 6.12: Recorded outlet, inlet temperature histories on March 29th

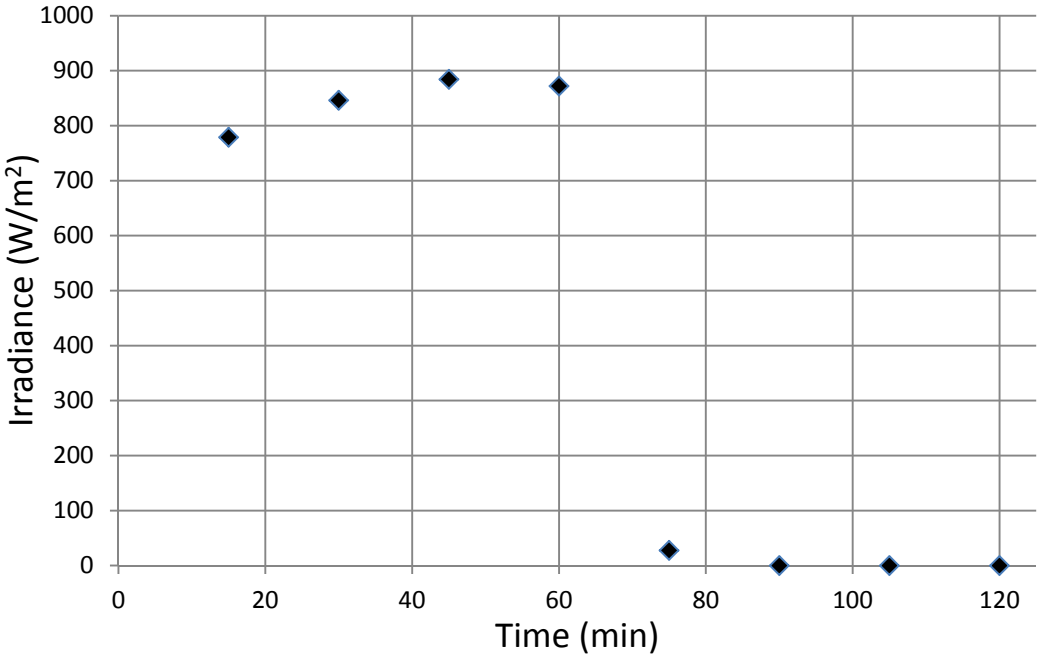

Figure 6.13: History of The recorded solar radiation on March 29th

Figure 6.14 compares the measured temperature histories at the inlet and outlet nodes collected on March 29th to the predicted values using the proposed numerical model. Again, the measured results agree well with the predictions. and computation results. The maximum error was 2.8% for the inlet temperature, and 4.5% for the outlet temperature. The measured data is presented in Appendix C

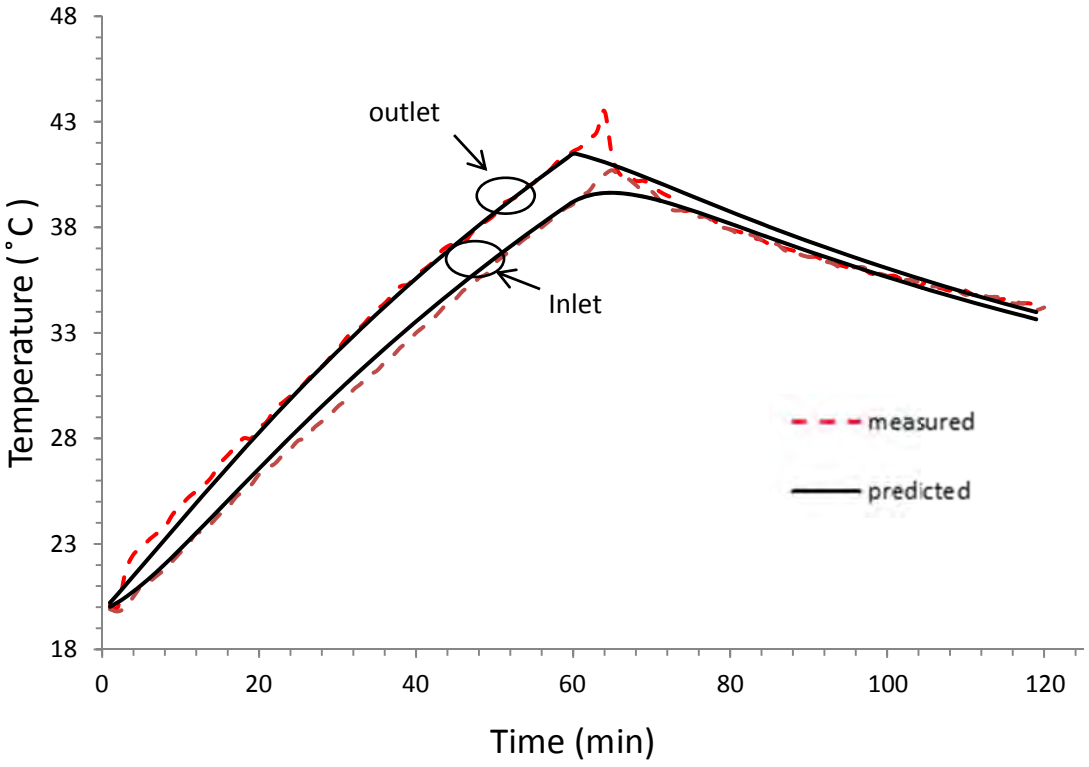

Figure 6.14: Comparison of measured and computed fluid temperatures histories at the solar collector inlet and outlet March 29th

CHAPTER 7- CONCLUSIONS AND RECOMMENDATIONS

7.1 Conclusions

On the basis of the results obtained in this study, the following conclusions can be drawn:

- A detailed mathematical derivation for the flat-plate solar collector cross sections (cover, air gap, absorber, working fluid, and insulation) was presented.
- A one dimensional mathematical model with distributed parameters that combines the solar collector's tank model and the flat-plat model is derived to simulate the collector process.
- All the thermo-physical properties of the air gap, the absorber plate, and the working fluid are computed in time dependent mode. The transient heat transfer coefficients are also computed in real time.
- To solve the derived system of equations, the implicit finite-difference scheme was suggested.
- The proposed method allows the transient processes occur in the flat-plate solar collector to be simulated. The time dependent flow rate, variable ambient temperature, and variable solar irradiance have been taken in consideration.

- The proposed solution method was implemented by utilizing the MATLAB software. The code mathematically solves the model and iteratively evaluates the temperature histories for each analyzed cross section of the solar collector at any selected point along the flow direction.
- The efficiency of the proposed method was confirmed by experimental verification. The analysis shows a very good agreement between the measured and the numerically predicted values for different running conditions and flow rates.
- The method solved some of the limitations in the existing models with distributed models. It does not require entering the inlet temperature history, it is appropriate for low and high flow rates operations.
- The code can be applied for verification of the effectiveness of various absorbers materials and their surface coating, as well as the cover materials, without the necessity of carrying out the experimental work.

7.2 Recommendations

- More experimental investigations are needed to confirm the efficiency of the proposed model, by testing the code for different cases.
- Use of insulated storage tank for the collector to minimize the approximation error in the ambient-tank free convection coefficient.
- Improving the running time of the code by using the inner product function instead of the loops.

LIST OF REFERENCES

LIST OF REFERENCES

[1] Anderson T., Duke M., and Carson J., 2010, The effect of color on the thermal performance of building integrated solar collectors, Solar Energy Materials & solar cells, 94, 350-354.

[2] Augustus M. and Kumar S., 2007, Mathematical modeling and thermal performance analysis of unglazed transpired solar collectors, Solar Energy, 81, 62-75.

[3] Cadafalch J., 2009, a detailed numerical model for flat-plate solar thermal devices, Solar Energy Vol. 83, pp. 2157-2164.

[4] Close D., 1967, A design approach for solar processes, Solar Energy, 11, 112.

[5] De Ron A., 1980, Dynamic modelling and verification of a flat-solar collector, Solar Energy, 24, 117-128.

[6] Duffie J. and Beckmann W., 1991, Solar engineering of thermal processes, 2nd edition (Wiley Interscience, New York).

[7] Duffie J. and Beckmann W., 2006, Solar engineering of thermal processes, 3rd edition (Wiley Interscience, New York).

[8] Fan J., Shah L., and Furbo S., 2007, Flow distribution in a solar collector panel with horizontally inclined absorber strips, Solar Energy, 81, 1501-1511.

[9] Farkas I., Geczy-Vig P., 2003, Neural network modelling of flat-plate solar collectors, Computers and electronics in Agriculture, 40, 87-102.

[10] Hilmer F., Vajen K., Ratka A., Ackermann H., Fuhs W., and Melsheimer O., 1998, Numerical solution and validation of a dynamic model of solar collectors working with varying fluid flow rate, Solar Energy Vol. 65, No. 5, pp. 305-321

[11] Hollands K., Unny T. Raithby G, and Konicek L., 1976, Free convective Heat Transfer Across Inclined Air Layers, Trans. of ASME : Journal of Heat Transfer vol. 190, pp. 189-193.

[12] Kalogirou S., 2006, Prediction of flat-plate collector performance parameters using artificial neural networks, Solar Energy, 80, 248-259.

[13] Kamminga W., 1985, the approximate temperatures within a flat-plate solar collector under transient conditions, Int. J. Heat Mass Transfer Vol. 28, No. 2, pp.433-440.

[14] Klein S., Duffie J., and Beckman W., 1974, Transient considerations of flat-plate solar collectors, Trans. of ASME: Journal Engineering for Power vol. 96A, pp. 109-113.

[15] Lawrence Livermore National Laboratory (LLNL), https://www.llnl.gov.

[16] Martinopoulos G., 2010, CFD modeling of a polymer solar collector, Renewable Energy Vol. 35, pp. 1499-1508.

[17] MathWorks inc. http://www.mathworks.com/products/MATLAB/.

[18] Micro Circuit Labs. (2010). SDL-1 Solar Data Logger: Assembly and Operating Manual. <www.microcircuitlabs.com>.

[19] Molero Villar N., Cejudo Lopez J., and Dominguez Munoz F., 2009, Numerical 3-D heat flux simulations on flat plate solar collectors, 83, 1086-1092.

[20] Muschaweck J. and Spirkl W., 1993, Dynamic solar collector performance testing, Solar Energy Materials and Solar Cells Vol. 30, pp.95-105.

[21] Oliva A., Costa M., and Perez Segarra C., 1991, Numerical simulation of solar collectors: the effect of nonuniform and nonsteady state of boundary conditions, Solar Energy, 47, 5, 359-373.

[22] RETScreen® International. (2012). Clean Energy Decision Support Centre. Clean Energy Project Analysis: RETScreen® Engineering & Cases Textbook. <www.retscreen.net>.

[23] Schnieders J., 1997, Comparison of the energy yield predictions of stationary and dynamic solar collector models and the models' accuracy in the description of a vacuum tube collector, Solar Energy, 61, 3, 179-190.

[24] Silicon Solar, Inc. (2008). SunMaxx Flat Plate Solar Collectors. Silicon Solar, Inc.: Innovative Solar Solutions.

[25] Singh P., Sarviya R., and Bhagoria J., 2010, Heat loss study of trapezoidal cavity absorbers for linear solar concentrating collector, Energy Convergence and Management, 51, 329-337.

[26] Srtuckmann, F. (2008). Project Report: MVK160 Heat and Mass Transport, May 08, 2008. Lund, Sweden.

[27] U.S Energy Information Administration, The Annual Energy Review 2010, http://www.eia.gov.

[28] Wang X. and Wu L., 1990, Analysis and performance of flat-plate solar collector arrays, solar energy, 45, 2, 71-78.

[29] Weitbrecht V., Lehmann D., and Richter A., 2002, Flow distribution in solar collectors with laminar flow conditions, Solar Energy, 73,6,433-441.

[30] Zima, Wieslaw and Dziewa, Piotr. (2010). Mathematical modeling of heat transfer in liquid flat-plate solar collector tubes. Archives of Thermodynamics, 31, 45–62.

[31] Zima W and Dziewa P , 2011, Modelling of liquid flat-plate solar collector operation in transient states, Proc. IMechE Part A: Journal of power and energy Vol. 225, pp. 53-62.

[32] Zueva G. and Magiera J., 2001, Mathematical model of heat transfer in solar collector and its experimental validation, Theoretical Foundations of Chemical Engineering, 35, 6, 604-608.

APPENDICES

Appendix A: MATLAB Code

```
function results(n,flowrate,interval,initialtemp,tankvol)
%n= number of nodes along the tube.
%flowrate= the total flow rate enter the system in GPM
%interval= total running time (min).
%initialtemp= initial temperature of the tank(C)
% tank volume in litters.

ts= cputime;                %time at the function start
d_in=9.5/1000;              %tube inner diameter
L=1900/1000;                %length of tubes
m_tank=tankvol;             % fluid mass in the tank (Kg)
flow=flowrate/8;            %fluid volume flow rate per tube (GPM)
Vdot=flow/15852;            %fluid volume flow rate (m^3/s)
mdot=Vdot*1000;             %fluid mass flow rate (Kg/s)
w_f=4*Vdot/(pi*d_in^2);     %working fluid velocity
dz=L/(n-1);                 %spatial step (m)
dtau=dz/w_f;                % maximum time step (s)
T_int=interval*60;          %total time interval(s)
T_tot= round(T_int/dtau);   %number of time steps
if dtau>dz/w_f
   fprintf('error in flow rate')
else
%%%%%%%%%%%%%%%%%%%%
tfile = 'ptemp.out';
fid = fopen(tfile,'wt');
count = fprintf(fid,'  number of nodes = %6.1f\n  flowrate(GPM) = %6.1f\n
interval(min) = %6.1f\n  initial temperature(C) = %6.1f\n  tank volume(L) = %6.1f\n
time step = %6.1f\n', n,flowrate,interval,initialtemp,tankvol,dtau);
count = fprintf(fid,'  time      irrad      T_tank      T_out      Q_out      T_g      T_a
T_ab      T_f      T_i      n_iter \n');
%%%%%%%%%%%%%%%%%%%%

t_am=zeros(T_tot+1,1);      %Ambient temp.
G_r=zeros(T_tot+1,1);       %Heat flux of solar radiation. (W/sqm)
t_g=ones(n,1)*293;          %initial glass temp.
t_a=ones(n,1)*293;          %initial air gap temp.
t_ab=ones(n,1)*293;         %initial absorber temp.
t_f=ones(n,1)*293;          %initial fluid temp.
t_i=ones(n,1)*293;          %initial insulation temp.

t_gc=zeros(T_tot,1);t_ac=zeros(T_tot,1);t_abc=zeros(T_tot,1);
t_fc=zeros(T_tot,1);t_ic=zeros(T_tot,1);t_out=zeros(T_tot,1);
```

```
Q_dot=zeros(T_tot,1);

t_tank=ones(T_tot,1)* (initialtemp+273);
counter=1;
for k=1:T_tot+1
   if k*dtau<=3600
        G_r(k)=660;
        t_am(k)=28+273.15;
   else
        G_r(k)=0;
        t_am(k)=28+273.15;
   end
end
for k = 1:T_tot
     n_converge=0;


[B,C,D,E,F,G,H,K,L,M,O,P,Q,R,S,U,V,W,X,J]=coeff(t_g,t_a,t_ab,t_f,t_i,t_am,dtau,dz,n
,mdot,k,w_f);

   kk = 0;
   while n_converge < 5*n
      kk = kk + 1;
      t_g_old=t_g;t_a_old=t_a;t_ab_old=t_ab;t_f_old=t_f;t_i_old=t_i;

t_g(1)=((t_g_old(1)/dtau)+(B(1)*t_am(k))+(C(1)*t_ab(1))+(D(1)*t_a(1))+(E(1)*G_r(k)
))/F(1);
      t_a(1)=((t_a_old(1)/dtau)+(G(1)*(t_g(1)+t_ab(1))))/H(1);

t_ab(1)=((t_ab_old(1)/dtau)+(K(1)*G_r(k))+(L(1)*t_g(1))+(M(1)*t_a(1))+(O(1)*t_f(1))
+(P(1)*t_i(1)))/Q(1);
      t_f(1)=t_tank(k);
      t_i(1)=((t_i_old(1)/dtau)+(V(1)*t_ab(1))+(W(1)*t_am(k)))/X(1);
      for j=2:n

t_g(j)=((t_g_old(j)/dtau)+(B(j)*t_am(k))+(C(j)*t_ab(j))+(D(j)*t_a(j))+(E(j)*G_r(k)))/F(
j);
         t_a(j)=((t_a_old(j)/dtau)+(G(j)*(t_g(j)+t_ab(j))))/H(j);

t_ab(j)=((t_ab_old(j)/dtau)+(K(j)*G_r(k))+(L(j)*t_g(j))+(M(j)*t_a(j))+(O(j)*t_f(j))+(P(j
)*t_i(j)))/Q(j);
         t_f(j)=((t_f_old(j)/dtau)+(R(j)*t_ab(j))+(S(j)*t_f(j-1)/dz))/U(j);
         t_i(j)=((t_i_old(j)/dtau)+(V(j)*t_ab(j))+(W(j)*t_am(k)))/X(j);
      end
```

```
      %check convergence
      ccc = 0;
      for j=1:n
         if ccc<=0
            error=zeros(5,1);
            error(1)=abs(t_g(j)-t_g_old(j))/t_g(j);
            error(2)=abs(t_a(j)-t_a_old(j))/t_a(j);
            error(3)=abs(t_ab(j)-t_ab_old(j))/t_ab(j);
            error(4)=abs(t_f(j)-t_f_old(j))/t_f(j);
            error(5)=abs(t_i(j)-t_i_old(j))/t_i(j);
            for i=1:5
               if (error(i)<=10^-4)
               n_converge=n_converge+1;
               else
                  ccc=1;
               end
            end
         end
      end
   end
   t_gc(k)= t_g(n/2);t_ac(k)= t_a(n/2);t_abc(k)= t_ab(n/2);
   t_fc(k)= t_f(n/2);t_ic(k)= t_i(n/2);t_out(k)= t_f(n);
   t_tank(k+1)= (mdot*8/m_tank)*1.0152*dtau*(t_out(k)-t_tank(k))-
(12*3*dtau*(t_tank(k)-t_am(k)))/(m_tank*4070)+t_tank(k);
   Q_dot(k)= mdot*4.186*(t_out(k)-t_tank(k));
   time = dtau*k/60;
   fprintf('time = %6.1f  T_tank = %8.2f     T_out = %8.2f     Q_out = %8.2f     T_g =
%8.2f    T_a = %8.2f     T_ab = %8.2f    T_f = %8.2f   T_i = %8.2f  n_iter =
%5.0f\n',time,t_tank(k),t_out(k),Q_dot(k),t_gc(k),t_ac(k),t_abc(k),t_fc(k),t_ic(k),kk);
   if time-counter >=0
      count = fprintf(fid,'%6.1f     %6.1f     %8.2f     %8.2f     %8.2f     %8.2f     %8.2f
%8.2f     %8.2f     %8.2f     %5.0f\n',time,G_r(k),t_tank(k),t_out(k),Q_dot(k),
t_gc(k),t_ac(k),t_abc(k),t_fc(k),t_ic(k),kk);
      counter=counter+1;
   end
end

fprintf('converged')
T=1:T_tot;
subplot(2,2,1)
plot(T,t_gc,T,t_ac,T,t_abc,T,t_fc,T,t_ic,T,t_am(1:T_tot))
subplot(2,2,2)
plot(T,t_tank(1:T_tot),T,t_out,T,t_fc)
subplot(2,2,3)
plot(T,Q_dot)
```

```
subplot(2,2,4)
plot(T,G_r(1:T_tot))
 runtime = cputime-ts
 count = fprintf(fid,'  run time = %6.1f\n',runtime);
 status = fclose(fid);
end


function[B,C,D,E,F,G,H,K,L,M,O,P,Q,R,S,U,V,W,X,J]=
coeff(t_g,t_a,t_ab,t_f,t_i,t_am,dtau,dz,n,mdot,k,w_f)

%Coefficients of the transiant temperature equations.
[p,d_in,r_o,r_in,A,delta_g,delta_i,delta_ab,delta_a,c_g,c_i,rho_g,rho_i,alpha,tau_alpha,
K_i,c_ab,rho_ab,c_a]= get_constants;
[h_g_am, h_r1, h_c1, h_f, h_i_am]=
get_h(t_f,t_a,t_g,t_ab,t_i,n,t_am,delta_a,d_in,k,w_f);
[rho_a] = rho(t_a);
[rho_f,c_f]= waterprop(t_f);
B=zeros(n,1);C=zeros(n,1);D=zeros(n,1);E=zeros(n,1);F=zeros(n,1);J=zeros(n,1);K=zer
os(n,1);L=zeros(n,1);M=zeros(n,1);O=zeros(n,1);
P=zeros(n,1);G=zeros(n,1);H=zeros(n,1);Q=zeros(n,1);R=zeros(n,1);S=zeros(n,1);U=ze
ros(n,1);V=zeros(n,1);W=zeros(n,1);X=zeros(n,1);

for j=1:n
   B(j)=h_g_am(j)/(c_g*rho_g*delta_g);
   C(j)=h_r1(j)/(c_g*rho_g*delta_g);
   D(j)=h_c1(j)/(c_g*rho_g*delta_g);
   E(j)=alpha/(c_g*rho_g*delta_g);
   F(j)=(1/dtau)+B(j)+C(j)+D(j);
   J(j)=c_ab*rho_ab*(p*delta_ab+pi*(r_o^2-r_in^2));
   K(j)=p*(tau_alpha)/J(j);
   L(j)=h_r1(j)*p/J(j);
   M(j)=h_c1(j)*p/J(j);
   O(j)=pi*d_in*h_f(j)/J(j);
   P(j)=p*K_i/(J(j)*delta_i);
   G(j)=h_c1(j)*p/(c_a*rho_a(j)*(p*delta_a-pi*r_o^2));
   H(j)=(1/dtau)+(2*G(j));
   Q(j)=(1/dtau)+L(j)+M(j)+O(j)+P(j);
   R(j)=pi*d_in*h_f(j)/(c_f(j)*rho_f(j)*A);
   S(j)=mdot/(rho_f(j)*A);
   U(j)=(1/dtau)+R(j)+(S(j)/dz);
   V(j)=2*K_i/(c_i*rho_i*delta_i^2);
   W(j)=2*h_i_am(j)/(c_i*rho_i*delta_i);
   X(j)=(1/dtau)+V(j)+W(j);
end
```

```
function
[p,d_in,r_o,r_in,A,delta_g,delta_i,delta_ab,delta_a,c_g,c_i,rho_g,rho_i,alpha,tau_alpha,
K_i,c_ab,rho_ab,c_a]= get_constants
p=.127;                    %tube pitch (m)
d_in=9.5/1000;               %tube inner diameter(m)
r_o=5/1000;                 %tube outer radius(m)
r_in=d_in/2;                %tube inner radius(m)
A=pi*r_in^2;                %flow area(sqm)
delta_g=3.81/1000;            %cover thickness
delta_i=50.8/1000;            %insulation thickness(m)
delta_ab=.015;              %absorber thickness(m)
delta_a=.025;               %air gap thickness(m)
c_g=720;                   %cover specific heat (J/kg.K)
c_i=1030;                  %insulation specific heat (J/kg.K)
rho_g=2500;                 %cover density(Kg/m^3)
rho_i=70;                  %insulation density(Kg/m^3)
alpha=.005;                %absorption coefficient;
tau_alpha=.861;              %effictive transmittance-absorption coef.
K_i=0.035;                 %insulation thermal conductivity(W/m.K)
c_ab =385;                 %absorber specific heat (J/kg.K)
rho_ab =8795;                %absorber density(Kg/m^3)
c_a=1.0056e+003;              %air specific heat (J/kg.K)

function [h_g_am, h_r1, h_c1, h_f, h_i_am]=
get_h(t_f,t_a,t_g,t_ab,t_i,n,t_am,delta_a,d_in,k,w_f)
[ny_a,alpha_a,k_a] = air_prop(t_a);
[k_f,ny_f,Pr_f]=kf(t_f);
Re_f=w_f.*d_in./ny_f;

segma=5.6697*10^-8;
emi_g=.88;emi_ab=.1;emi_i=.05;
g=9.81;
theta=(pi/4);              % tilt angle
a=1.9;b=.92;L=a;             % collector dimensions
U_inf=1.5;                 % wind velocity
%
h_f=zeros(n,1);h_r1=zeros(n,1);h_c1=zeros(n,1);h_g_am=zeros(n,1);
h_i_am=zeros(n,1);Nu_f=zeros(n,1);Nu_a=zeros(n,1);Ra=zeros(n,1);
ny_am =1.5743*10^-5;
k_am=.0262;                %ambiant thermal conductivity
Pr_am=0.71432;               %ambiant Prandtl number

delta=4*a*b/sqrt(a^2+b^2);
Re_am=U_inf*delta/ny_am;
```

```
Nu_am=.86*Re_am^.5*Pr_am^(1/3);
h_c2=Nu_am*k_am/delta;
%
t_sky=.0552.*t_am.^1.5;
Nu_f=4.4+(.00398.*(Re_f.*Pr_f.*(d_in/L)).^1.66./(1+.0114.*(Re_f.*Pr_f.*(d_in/L)).^1.
12));
h_f=Nu_f.*k_f./d_in;

for j=1:n
   Ra(j)=abs(t_g(j)-t_ab(j))*g*delta_a^3/(ny_a(j)*alpha_a(j)*t_a(j));
   AA=1-(1708/(Ra(j)*cos(theta)));
   BB=(Ra(j)*cos(theta)/5830)^(1/3)-1;
   if AA<=0
      if BB<=0
         Nu_a(j)=1;
      else Nu_a(j)=1+BB;
      end
   else if BB<=0
         Nu_a(j)=1+(1.44*(1-(1708*(sin(1.8*theta))^1.6/(Ra(j)*cos(theta))))*AA);
      else Nu_a(j)=1+(1.44*(1-(1708*(sin(1.8*theta))^1.6/(Ra(j)*cos(theta))))*AA)+BB;
      end
   end
   h_r1(j)=(segma*(t_ab(j)^2+t_g(j)^2)*(t_ab(j)+t_g(j)))/((1/emi_ab)+(1/emi_g)-1);
   h_c1(j)=Nu_a(j)*k_a(j)/delta_a;
   if t_g(j)-t_am(k)==0
      h_g_am(j)=h_c2;
   else
      h_g_am(j)=((segma*emi_g*(t_g(j)^4-t_sky(k)^4))/(t_g(j)-t_am(k)))+h_c2;
   end
   if t_i(j)-t_am(k)==0
      h_i_am=h_c2;
   else
      h_i_am(j)=((segma*emi_i*(t_i(j)^4-t_sky(k)^4))/(t_i(j)-t_am(k)))+h_c2;
   end


end
function [ny_a,alpha_a,k_a] = air_prop(t_a)
T_vec = [250 300 350 400 450];
ny_vec = [11.44 15.89 20.92 26.41 32.39]*1E-6;
alpha_vec = [15.9 22.5 29.9 38.3 47.2]*1E-6;
ka_vec = [22.3 26.3 30.0 33.8 37.3]*1E-3;
ny_a = interp1(T_vec,ny_vec,t_a,'spline');
alpha_a = interp1(T_vec,alpha_vec,t_a,'spline');
k_a = interp1(T_vec,ka_vec,t_a,'spline');
```

```
function [rho_a] = rho(t_a)
T_vec = [250 300 350 400 450];
rho_vec = [1.4235 1.1771 1.0085 0.88213 .8770];
rho_a=interp1(T_vec,rho_vec,t_a,'spline');

function [k_f,ny_f,Pr_f]=kf(t_f)
T_vec = [273.15 300 350];
kf_vec = [0.57214 0.61497 0.66786 ];
nyf_vec = [1.6438E-6 8.3610E-7 3.6987E-7];
Prf_vec = [11.822 5.5141 2.1929];
k_f = interp1(T_vec,kf_vec,t_f,'spline');
ny_f = interp1(T_vec,nyf_vec,t_f,'spline');
Pr_f = interp1(T_vec,Prf_vec,t_f,'spline');

function [rho_f,c_f]= waterprop(t_f)
T_vec = [273.15 300 350];
rhof_vec = [1000.4 996.75 973.8];
cf_vec = [4112.9  4071.7 4068.5];
rho_f = interp1(T_vec,rhof_vec,t_f,'spline');
c_f = interp1(T_vec,cf_vec,t_f,'spline');
```

Appendix B: Data Collected on March 22nd

Table B.1: Measured solar irradiance and ambient temperature on March 22nd

Index	Time (min)	10 x [Irradiance (W/m^2)]	Irradiance (W/m^2)	Temperature (˚F)	Temperatures (˚C)
0	0	0	0	75	23.89
1	15	8496	849.6	95	35.00
2	30	8582	858.2	102	38.89
3	45	8961	896.1	107	41.67
4	60	8910	891	109	42.78
5	75	1775	177.5	96	35.56
6	90	0	0	88	31.11
7	105	0	0	84	28.89
8	120	0	0	82	27.78

Table B.2: Measured temperatures on March 22nd

Time (min)	T_{in} (˚C)	T_{out} (˚C)	Time (min)	T_{in} (˚C)	T_{out} (˚C)	Time (min)	T_{in} (˚C)	T_{out} (˚C)
1	23.6	26.1	13	30.2	33.1	25	36.4	39.8
2	24.3	26.8	14	30.7	33.6	26	36.9	40.3
3	24.7	27.2	15	31.3	34.2	27	37.5	40.8
4	25.2	28	16	31.8	34.9	28	37.9	41.4
5	25.6	28.5	17	32.5	35.3	29	38.3	41.8
6	26.1	29.1	18	32.9	35.8	30	38.8	42.4
7	26.8	29.6	19	33.5	36.3	31	39.3	42.8
8	27.2	30.2	20	34	37	32	39.7	43.3
9	27.9	30.8	21	34.4	37.8	33	40.2	43.8
10	28.5	31.4	22	35	38.5	34	40.6	44.1
11	29.1	32	23	35.4	38.9	35	41	44.5
12	29.7	32.5	24	35.8	39.4	36	41.3	44.9

Time (min)	T_{in} (˚C)	T_{out} (˚C)	Time (min)	T_{in} (˚C)	T_{out} (˚C)	Time (min)	T_{in} (˚C)	T_{out} (˚C)
37	41.7	45.2	71	48.3	48	105	42.2	41.8
38	42.1	45.5	72	48.2	47.8	106	42.1	41.6
39	42.5	45.8	73	48	47.6	107	41.9	41.3
40	42.8	46.3	74	47.7	47.3	108	41.8	41.2
41	43.2	46.6	75	47.5	47.2	109	41.5	41.1
42	43.6	47.1	76	47.4	47	110	41.3	41.1
43	44.1	47.7	77	47.2	46.8	111	41.3	40.8
44	44.5	48.2	78	46.9	46.6	112	41.2	40.7
45	44.7	48.8	79	46.8	46.3	113	41.1	40.7
46	45.5	49.1	80	46.6	46.1	114	41	40.5
47	45.8	49.6	81	46.2	45.8	115	40.8	40.4
48	46.3	49.9	82	46.1	45.5	116	40.8	40.2
49	46.6	50.4	83	45.8	45.5	117	40.6	40.1
50	47.1	50.8	84	45.7	45.3	118	40.5	40
51	47.4	51.2	85	45.5	45.1	119	40.3	39.8
52	47.7	51.6	86	45.2	45	120	40.2	39.8
53	48.1	51.8	87	45.2	44.7			
54	48.3	52.2	88	44.9	44.6			
55	48.6	52.3	89	44.7	44.3			
56	49.1	52.5	90	44.5	44.1			
57	49.1	53.1	91	44.3	44			
58	49.3	53.2	92	44.1	43.8			
59	49.5	53	93	43.9	43.6			
60	49.7	53.2	94	43.8	43.6			
61	50.1	53.3	95	43.6	43.3			
62	50.2	54.2	96	43.5	43.2			
63	50.3	51.8	97	43.6	43			
64	50.1	50	98	43.2	42.8			
65	49.7	49.5	99	43	42.7			
66	49.6	49.2	100	43	42.5			
67	49.2	49	101	42.7	42.3			
68	49.1	48.7	102	42.6	42.2			
69	48.8	48.5	103	42.5	42.1			
70	48.6	48.2	104	42.2	41.8			

Appendix C: Data Collected on March 29nd

Table C.1: Measured solar irradiance and ambient temperature on March 29th

Index	Time (min)	10 x [Irradiance (W/m^2)]	Irradiance (W/m^2)	Temperature (˚F)	Temperatures (˚C)
0	0	792	79.2	61	16.11
1	15	7790	779	77	25.00
2	30	8462	846.2	85	29.44
3	45	8841	884.1	88	31.11
4	60	8720	872	90	32.22
5	75	275	27.5	74	23.33
6	90	0	0	71	21.67
7	105	0	0	71	21.67
8	120	0	0	71	21.67

Table C.2: Measured temperatures on March 29th

Time (min)	T_{in} (˚C)	T_{out} (˚C)	Time (min)	T_{in} (˚C)	T_{out} (˚C)	Time (min)	T_{in} (˚C)	T_{out} (˚C)
1	20.2	20.1	13	23.8	25.8	25	28	30.3
2	20.3	20	14	24.1	26.2	26	28.3	30.7
3	20.3	21.7	15	24.3	26.8	27	28.6	31.1
4	20.6	22.5	16	24.7	27.2	28	29	31.4
5	20.8	22.8	17	25	27.6	29	29.3	31.8
6	21.1	23.2	18	25.4	28	30	29.7	32.2
7	21.5	23.5	19	25.8	28	31	30.1	32.7
8	21.6	23.8	20	26.1	28.5	32	30.5	33.1
9	22.1	24.4	21	26.6	28.8	33	31	33.3
10	22.4	24.8	22	26.9	29.4	34	31.4	33.7
11	22.8	25.2	23	27.2	29.7	35	31.6	34.1
12	23.3	25.5	24	27.7	30	36	31.9	34.4

Time (min)	T_{in} (˚C)	T_{out} (˚C)	Time (min)	T_{in} (˚C)	T_{out} (˚C)	Time (min)	T_{in} (˚C)	T_{out} (˚C)
37	32.3	34.8	72	40.2	39.5	107	35.4	35.1
38	32.5	35.2	73	39.8	39.3	108	35.3	35
39	33.1	35.3	74	39.6	38.8	109	35.2	35.1
40	33.5	35.7	75	39.4	38.8	110	35	35
41	33.6	36	76	39.2	38.6	111	35.2	34.8
42	33.8	36.3	77	39.1	38.5	112	34.8	34.8
43	34.1	36.8	78	38.8	38.3	113	34.9	34.7
44	34.3	37.1	79	38.6	38	114	34.8	34.6
45	34.7	37.2	80	38.3	37.9	115	34.6	34.6
46	35.1	37.2	81	38.2	37.8	116	34.6	34.6
47	35.5	37.7	82	38	37.7	117	34.5	34.4
48	35.8	38.1	83	38	37.5	118	34.4	34.4
49	36.1	38.3	84	37.7	37.4	119	34.6	34.3
50	36.5	38.6	85	37.5	37.2	120	34.3	34.1
51	36.8	39.1	86	37.4	37.1			
52	37.1	39.3	87	37.2	37			
53	37.5	39.5	88	37.1	36.9			
54	37.7	39.9	89	37.1	36.8			
55	38.1	40.1	90	37	36.6			
56	38.5	40.5	91	36.9	36.6			
57	38.9	40.7	92	36.8	36.4			
58	39.1	41.1	93	36.6	36.3			
59	39.4	41.3	94	36.5	36.2			
60	39.6	41.6	95	36.4	36.1			
61	39.7	41.8	96	36.3	36			
62	40.2	42.2	97	36.1	36			
63	40.3	42.5	98	36.1	35.8			
64	40.5	43.5	99	36.1	35.8			
65	41	41.3	100	35.8	35.7			
66	41	40.5	101	35.8	35.7			
67	41.2	40.5	102	35.8	35.5			
68	41.1	40.2	103	35.8	35.5			
69	40.8	40.2	104	35.5	35.2			
70	40.7	40	105	35.4	35.4			